

JGR Atmospheres

RESEARCH ARTICLE

10.1029/2018JD029501

Key Points:

- Two co-located types of ambient brown carbon were characterized, one from biomass combustion and one from secondary aerosol formation
- Limited mixing-induced absorption enhancement observed in two distinct environments, despite substantial average coatings on black carbon

Supporting Information:

- Supporting Information S1

Correspondence to:

C. D. Cappa,
cdcappa@ucdavis.edu

Citation:

Cappa, C. D., Zhang, X., Russell, L. M., Collier, S., Lee, A. K. Y., Chen, C.-L., et al. (2019). Light absorption by ambient black and brown carbon and its dependence on black carbon coating state for two California, USA, cities in winter and summer. *Journal of Geophysical Research: Atmospheres*, 124, 1550–1577. <https://doi.org/10.1029/2018JD029501>

Received 15 AUG 2018

Accepted 27 DEC 2018

Accepted article online 7 JAN 2019

Published online 1 FEB 2019

Light Absorption by Ambient Black and Brown Carbon and its Dependence on Black Carbon Coating State for Two California, USA, Cities in Winter and Summer

Christopher D. Cappa¹ , Xiaolu Zhang^{1,2} , Lynn M. Russell³ , Sonya Collier^{4,5} , Alex K. Y. Lee⁶ , Chia-Li Chen³ , Raghu Betha³ , Sijie Chen³ , Jun Liu³ , Derek J. Price^{3,7} , Kevin J. Sanchez³ , Gavin R. McMeeking⁸ , Leah R. Williams⁹ , Timothy B. Onasch⁹ , Douglas R. Worsnop⁹ , Jon Abbatt¹⁰ , and Qi Zhang⁴ 

¹Department of Civil and Environmental Engineering, University of California, Davis, CA, USA, ²Now at IMPROVE, University of California, Davis, CA, USA, ³Scripps Institution of Oceanography, University of California, San Diego, CA, USA, ⁴Department of Environmental Toxicology, University of California, Davis, CA, USA, ⁵Now at California Air Resources Board, Sacramento, CA, USA, ⁶Department of Civil and Environmental Engineering, National University of Singapore, Singapore, ⁷Now at Cooperative Institute for Research in Environmental Sciences, University of Colorado Boulder, Boulder, CO, USA, ⁸Handix Scientific, Boulder, CO, USA, ⁹Aerodyne Research, Inc., Billerica, MA, USA, ¹⁰Department of Chemistry, University of Toronto, Toronto, Ontario, Canada

Abstract Observations from a wintertime and summertime field campaign are used to assess the relationship between black and brown carbon (BC and BrC, respectively) optical properties and particle composition and coating state. The wintertime campaign, in Fresno, CA, was impacted by primary emissions from residential wood burning, secondary organic and inorganic particle formation, and BC from motor vehicles. Two major types of BrC were observed in wintertime. One occurred primarily at night—the result of primary biomass burning emissions. The second was enhanced in daytime and strongly associated with particulate nitrate and the occurrence of fog. The biomass-burning-derived BrC absorbed more strongly than the nitrate-associated BrC but had a weaker wavelength dependence. The wintertime BC-specific mass absorption coefficient (MAC_{BC}) exhibited limited dependence on the ensemble-average coating-to-BC mass ratio ($R_{coat-rBC}$) at all wavelengths, even up to $R_{coat-rBC}$ of ~ 5 . For the summertime campaign, in Fontana, CA, BC dominated the light absorption, with negligible BrC contribution even after substantial photochemical processing. The summertime MAC_{BC} exhibited limited dependence on $R_{coat-rBC}$, even up to ratios of >10 . Based on the four classes of BC-containing particles identified by Lee et al. (2017, <https://doi.org/10.5194/acp-17-15055-2017>) for the summertime measurements, the general lack of an absorption enhancement can be partly—although not entirely—attributed to an unequal distribution of coating materials between the BC-containing particle types. These observations demonstrate that in relatively near-source environments, even those impacted by strong secondary aerosol production, the ensemble-average, mixing-induced absorption enhancement for BC due to coatings can be quite small.

Plain Language Summary Particles in the atmosphere can scatter light, which has a cooling effect, or absorb light, which can contribute to localized atmospheric warming. Black carbon is a highly absorbing yet short-lived climate pollutant that when coated with other materials can in theory have enhanced absorption. Organic compounds in particles can also absorb light, although tend to absorb less strongly than black carbon. Absorbing organic compounds are collectively referred to as brown carbon. We measured the composition and light absorption properties of atmospheric particles in wintertime Fresno, CA, and summertime Fontana, CA. In Fresno, we found two types of brown carbon contributed significantly to the overall light absorption by particles, in addition to absorption by black carbon. One of the brown carbon aerosol types in Fresno was emitted during wood burning, and the other was produced from chemical reactions in the atmosphere. In summertime Fontana, black carbon particles dominated the light absorption, with little contribution from brown carbon. Overall, at both sites the coating of materials onto black carbon particles had a limited impact on the absorption by black carbon, except to the extent that the materials themselves were absorbing.

1. Introduction

Light-absorbing aerosol particles influence climate through their ability to absorb solar and, to a lesser extent, longwave radiation. Light absorption by particles contributes a substantial, positive radiative forcing (Bond et al., 2013; Ramanathan & Carmichael, 2008). However, the uncertainty in global and regional radiative forcing by light-absorbing particles remains large. Two key light-absorbing particle types are black carbon (BC; Lack et al., 2014) and light-absorbing organic carbon, commonly referred to as brown carbon (BrC; Kirchstetter et al., 2004). BC absorbs strongly across the solar spectrum, whereas the absorptivity of BrC falls off rapidly as wavelength increases (Andreae & Gelencser, 2006).

Light absorption by BC depends on the particle mixing state that is the extent to which the BC is internally mixed with other materials, including BrC. Theoretically, when BC is internally mixed with (i.e., *coated* by) nonabsorbing materials, the absorption by the BC is increased (Bond et al., 2006; Fuller et al., 1999; Lack & Cappa, 2010). This mixing-induced enhancement, commonly (yet inaccurately) referred to as the *lensing*-based absorption enhancement, has been observed in various laboratory studies using controlled, typically monodisperse, BC sources (Cappa et al., 2012; Cross et al., 2010; Lack et al., 2009; Metcalf et al., 2013; Peng et al., 2016; Schnaiter et al., 2005; Shiraiwa et al., 2010). The mixing-induced absorption enhancement can be defined as $E_{\text{abs}} = b_{\text{abs,coat}}/b_{\text{abs,BC}}$, where $b_{\text{abs,coat}}$ and $b_{\text{abs,BC}}$ are the absorption coefficients for coated and uncoated BC, respectively. This definition implies no contributions from other absorbing components (e.g., BrC), although it should be noted that the observable E_{abs} can be influenced by absorbing components that are either internally or externally mixed from BC. The observed magnitude of E_{abs} in at least some of these studies has been reasonably consistent with theoretical calculations performed using Mie theory that is extended to treat BC-containing particles as having a core-shell morphology (Cappa et al., 2012). (We will refer to Mie theory extended to treat coated spheres as extended Mie theory or core-shell Mie theory.) However, field studies have resulted in a variety of often contradictory results. Some studies have observed relatively large E_{abs} , while others have not (Cappa et al., 2012; Healy et al., 2015; Knox et al., 2009; Krasowsky et al., 2016; Lim et al., 2018; Liu, Aiken, et al., 2015; Liu et al., 2017; Zhang et al., 2018). Some of this variability is probably due to methodological differences related to the measurement of E_{abs} , while some is likely due to uncharacterized differences in the particle mixing state (i.e., extent of coating) between studies as the relative amount of coating material is explicitly characterized in only a few of these studies. However, some field studies have simultaneously characterized E_{abs} (or a closely related property, the BC mass absorption coefficient, $\text{MAC}_{\text{BC}} = b_{\text{abs,obs}}/[\text{BC}]$) and the particle coating state, and we focus on these studies here as they provide stronger process-level constraints on the relationship between particle composition and absorption.

One method to characterize particle coating state uses the soot particle aerosol mass spectrometer (SP-AMS). The SP-AMS can measure the ensemble-average coating-to-core mass ratio ($R_{\text{coat-rBC}} = [\text{coating}]/[\text{BC}]$) of BC-containing particles, as well as the composition-dependent size distribution of these internally mixed particles (Massoli et al., 2015; Onasch et al., 2012). Recent developments have enabled determination of particle-to-particle differences in coating amount and composition with the SP-AMS (Lee et al., 2015; Lee et al., 2016; Willis et al., 2016). For reference, extended Mie theory predicts an approximately continuous increase in E_{abs} with $R_{\text{coat-rBC}}$ up to a plateau of $E_{\text{abs}} \sim 2.5$ when $R_{\text{coat-rBC}}$ is greater than ~ 30 , with substantial enhancements, on the order of 1.5, predicted for $R_{\text{coat-rBC}}$ values as small as 3. (The exact relationship between E_{abs} and $R_{\text{coat-rBC}}$ depends on the core BC diameter and the wavelength.) Cappa et al. (2012) used SP-AMS measurements to relate the magnitude of the absorption enhancement to the ensemble-average $R_{\text{coat-rBC}}$, as well as to theoretical calculations based on these bulk average measurements. Their measurements were made in summertime in the coastal region around California, USA, including well downwind of a major BC source region with high photochemical activity, that is, Los Angeles, CA. They observed that the ensemble-averaged absorption enhancement was negligible ($E_{\text{abs}} < 1.1$, on average, at 532 nm) even when the ensemble-average coating amount was substantial (up to $R_{\text{coat-rBC}} \sim 12$), and the observed E_{abs} were much lower than that predicted from extended Mie theory based on the coating amount. Healy et al. (2015) made measurements in downtown Toronto, Canada, and observed generally negligible E_{abs} at 781 nm even while $R_{\text{coat-rBC}}$ ranged from approximately 2–10, including for a period identified as being strongly impacted by wildfire emissions. McMeeking et al. (2014) made measurements of freshly

produced particles from open biomass combustion and observed negligible enhancement at 781 nm until the $R_{\text{coat-rBC}}$ was greater than 10.

In contrast, Liu, Aiken, et al. (2015) made measurements in a rural city near London and observed reasonably large BC absorption enhancement (up to ~ 1.5 at 870 nm) when the $R_{\text{coat-rBC}}$ values were only as large as ~ 5 , and the observed E_{abs} were reasonably consistent with SP-AMS observationally constrained extended Mie calculations. Peng et al. (2016) performed an experiment that combined laboratory with field measurements, allowing for secondary material formation from ambient air (in Beijing, China, or Houston, TX, USA) onto monodisperse proxy BC seeds. They observed that E_{abs} at 405 and 532 nm generally increased as coatings on the seed BC particles grew, although there was some evidence of an incubation period in which some minimum amount of particle growth must occur before the E_{abs} increases substantially. In a similar type of experiment, Tasoglou et al. (2017) observed that when BC particles derived from combustion of pine and birch were photochemically aged, the observed E_{abs} increased. Liu, Scheuer, et al. (2015) made ambient measurements at a London urban site and used an alternative method to estimate the BC coating amount and relate it to E_{abs} (or more specifically, the MAC_{BC}), namely, they inferred the BC coating thickness of single particles based on measurements made using a single particle soot photometer (SP2). Liu, Scheuer, et al. (2015) classified their observations into different regimes dependent upon the relative contribution of BC from solid fuel combustion versus traffic; the coating thickness was larger for BC from solid fuel combustion than from traffic. They observed a moderate increase in the MAC_{BC} at 781 nm as the average coating thickness (and solid fuel fraction) increased; the MAC_{BC} increased by a factor of 1.28 when the total particle-to-BC-only diameter ratio was ~ 2 (which corresponds to an $R_{\text{coat-rBC}} \sim 5$). The observations discussed above are summarized in Figure 1. Clearly, there is a great deal of variability between studies that aim to directly relate observed E_{abs} values to the particle coating state, and additional measurements in a variety of environments are needed.

In addition to BC, BrC can contribute substantially to regional and global radiative forcing. BrC is not one easily classifiable substance as it depends on the specific chemical nature of the organic compounds present, which in turn depends on the source and atmospheric transformations. As such, characterization of light absorbing properties of BrC in a range of environments is necessary to understand the extent to which different sources and processes are important to determining the atmospheric impacts of BrC and to allow for incorporation of BrC into climate models. One challenge in characterizing BrC properties is that the BrC absorption must be separated from BC absorption, including any coating-enhancement effect. One method to perform this separation is to extract the organic material into a solvent (e.g., water or methanol) and then to characterize the absorptivity of the extract (Kirchstetter et al., 2004; Liu et al., 2013; Liu, Taylor, et al., 2015; Zhang et al., 2013). This method has demonstrated that BrC absorption typically has a very strong wavelength dependence, characterized by a large absorption Ångstrom exponent (AAE), much greater than unity. A large AAE indicates a very strong wavelength dependence to absorption. (The AAE is the power exponent for the wavelength dependence of absorption, and an AAE of one [weak wavelength dependence] is typically attributed to BC, while an AAE in excess of two is characteristic of BrC [strong wavelength dependence].) Other methods have relied on attribution methods, typically either via optical closure (Cappa et al., 2012; Lack, Richardson, et al., 2012; Liu, Scheuer, et al., 2015; Liu, Aiken, et al., 2015; Zhang et al., 2016) or subtraction of inferred BC absorption (Lack & Langridge, 2013; Saleh et al., 2013; Saleh et al., 2014) or some combination of the two methods. Estimates of the MAC for BrC (or of the related imaginary refractive index, k) are variable, most likely as a result of a combination of real chemical differences (Lewis et al., 2008; Saleh et al., 2013; Saleh et al., 2014) and of imprecise understanding of which components of the total organic matter are responsible for the absorption (Andreae & Gelencser, 2006). One major global source of BrC is thought to be biomass combustion (Feng et al., 2013; Wang et al., 2014), as this is a major source of organic matter and biomass combustion-derived particles tend to be light absorbing, at least at shorter wavelengths ($\lesssim 600$ nm). BrC properties from biomass combustion-produced particles can be determined from laboratory studies involving intentional burns (Chakrabarty et al., 2010; McMeeking et al., 2014; Saleh et al., 2013; Saleh et al., 2014) or from analysis of field observations (Clarke et al., 2007; Forrister et al., 2015; Kirchstetter et al., 2004; Lack, Richardson, et al., 2012; Zhang et al., 2016).

In the current study, we report on measurements of light absorption by ambient particles made concurrent with BC ensemble-average coating state (via SP-AMS) and ensemble-average total particle composition. We

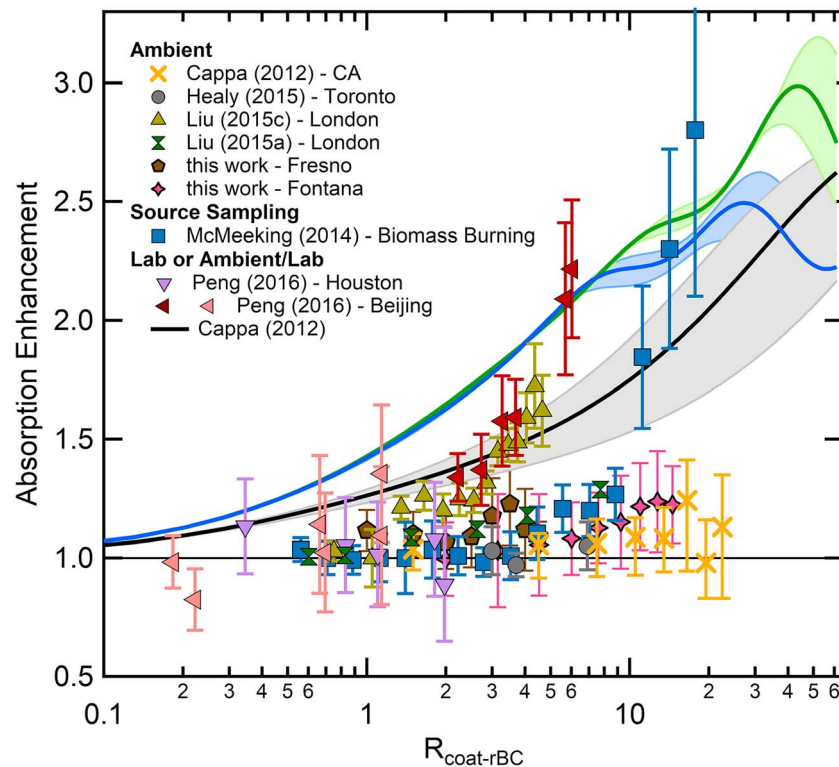


Figure 1. Compilation of various absorption enhancement measurements from ambient studies (Cappa et al., 2012; Healy et al., 2015; Liu, Scheuer, et al., 2015; Liu, Aiken, et al., 2015), including this work, from source sampling of biomass burning particles (McMeeking et al., 2014), and from lab (Cappa et al., 2012) or combined ambient/lab measurements (Peng et al., 2016). For all studies, the enhancements observed at the longest reported wavelength are used. For Liu, Scheuer, et al. (2015), the reported overall coating thickness ratio was used to calculate an equivalent $R_{\text{coat-rBC}}$, and the reported MAC values at 781 nm were converted to absorption enhancement values by dividing by the lowest observed value ($4 \text{ m}^2/\text{g}$). For Peng et al. (2016), the reported change in coating thickness was used to calculate an equivalent $R_{\text{coat-rBC}}$, and the different symbols for the same location correspond to measurements made on different days. For the lab experiments of Cappa et al. (2012), only the fit lines are shown, with different colors corresponding to experiments with different size particles. The error bars correspond to either a propagated uncertainty (Peng et al., 2016) or a standard deviation of the observations (all other studies).

use these measurements to assess the relationship between observed light absorption coefficients and the BC mixing state along with the contribution from BrC. The measurements were made during two independent campaigns, within distinctly different environments. One set of measurements was made in wintertime Fresno, CA. Detailed analyses of the bulk particle composition and the BC-containing particle composition measurements from this campaign are presented in Chen et al. (2018) and Collier et al. (2018), respectively. Wintertime Fresno is strongly impacted by emissions from biomass combustion, predominantly from residential fireplaces operating at night, and from secondary nitrate and organic aerosol (OA; Ge et al., 2012; Young et al., 2016; Zhang et al., 2016). This gives rise to a very strong diurnal variation in the ambient concentration of biomass-burning-derived OA compared to secondary components and in the wavelength-specific absorption enhancement. In a previous study, conducted in a different year, we used this diurnal variability to estimate the properties of BrC and the relationship between source and E_{abs} (Zhang et al., 2016). However, this previous study lacked knowledge of the BC mixing state and relative coating amount. The addition of particle coating measurements and mixing state characterization here allows for a more robust assessment of the E_{abs} and BrC measurements in terms of the primary controlling factors.

The second set of measurements was made in summertime Fontana, CA. Fontana is located inland in the South Coast Air Basin that includes the megacity Los Angeles. Measurements of ensemble-average particle composition are presented in Chen et al. (2018), and BC-containing particle composition and mixing state are discussed in Lee et al. (2017). The South Coast Air Basin is a highly photochemically active

environment in the summertime, with much of the particulate matter being secondary in origin (Docherty et al., 2008; Hayes et al., 2013), especially material that is internally mixed with BC (Cappa et al., 2012; Lee et al., 2017). Biomass burning contributions in this region are sporadic, depending on the occurrence of wild fires. Thus, the Fontana site measurements provide a complementary assessment of the relationship between absorption enhancement and BC mixing state and coating amount.

2. Methods

2.1. Campaign Overview

The measurements reported here were made from 25 December 2014 to 12 January 2015 in Fresno, CA, and from 3 July 2015 to 25 July 2015 in Fontana, CA. The Fresno measurement site was located at the University of California Center (36.810, -119.778). The average temperature and relative humidity (RH) were 13.5 °C and 60% during daytime and 6.4 °C and 81% during nighttime. The Fontana site was managed by South Coast Air Quality Management District and located behind the fire station at 14360 Arrow Highway (34.100, -117.490). The temperatures ranged from 15 to 36 °C, and the average RH was 52%. Further details regarding the meteorology during both campaigns are discussed in Chen et al. (2018). Figure S1 in the supporting information shows a map of CA with the locations of the two sites. In both studies all instruments were housed in a temperature-regulated modified shipping container (the *van*). Air was sampled into the van from 8 m above the ground, through a mast that extended 5 m above the ~ 3 -m-tall van. The mast had a horizontal inlet nozzle that could rotate into the relative wind so as to maintain an approximately isokinetic flow and to minimize the loss of particles. The flow through the mast was 1 m³/min. Twenty-one 1.6-cm outer diameter stainless steel tubes extended into the mast, and air was sampled from the mast through these tubes (not all were used). Air was sampled at 16.7 lpm through a diffusion drier packed with silica gel and then through a PM₁ cyclone. After the cyclone, the flow was split and 2.1 lpm was sampled through a custom thermodenuder with air passing alternatively through a heated channel ($T = 250$ °C) or a channel maintained at room temperature (i.e., the bypass) on a 5-min cycle. Part of both the heated and bypass channels were lined with charcoal cloth to scavenge NO₂. The airstream was then passed through a second diffusion drier after which the flow was split into three approximately equal streams. Air from one of these streams was sent to a single particle soot photometer (SP2, Droplet Measurement Technologies) and to a scanning electrical mobility sizer (SEMS, Brechtel Manufacturing, Inc.). The second stream went to the University of California (UC) Davis dual-wavelength cavity ringdown/photoacoustic spectrometer (CRD-PAS) and a particle absorption eXtinctionometer (PAX, Droplet Measurement Technologies). The third stream went to a SP-AMS (Aerodyne Research, Inc.) and a high-resolution aerosol mass spectrometer (HR-AMS, Aerodyne Research Inc.). A schematic of the instrument configuration is provided in Figure S2. Instrument details are provided in the sections that follow.

2.2. Refractory Black Carbon Measurement

Refractory black carbon (rBC; Lack et al., 2014) concentrations and BC-specific particle size distributions were measured using the SP2 instrument at both the Fresno and Fontana sites. While the operation of the SP2 has been previously discussed for these studies (Betha et al., 2018), further details are provided here and in Appendix A. The SP2 measures the concentration of rBC within individual rBC-containing particles. Sampled particles pass through a 1,064-nm intracavity laser. Absorption of this light by rBC leads to rapid heating of the particles. If heating outweighs conductive cooling, the particles will reach a sufficiently high temperature (i.e., their boiling point) that they will incandesce. The intensity of this incandescent light is proportional to the rBC mass of that particle (usually on the order of 0.1–10 fg per particle). Size distributions of only the rBC (exclusive of any other internally mixed material) are generated by converting the per particle mass to a volume equivalent diameter ($d_{p,VED}$ here, assuming $\rho_{rBC} = 1.8$ g/cm³) and binning the particles by size.

When the number concentration of rBC-containing or non-rBC-containing particles is large, the SP2 may suffer from negative biases in the concentration measurement. This can happen when the SP2 detectors are triggered by one particle and a second passes through the viewing volume during the detection window (typically ~ 50 μ s). Such particle coincidence effects can be minimized by decreasing the sample flow rate into the SP2 to decrease the likelihood that two particles are simultaneously in the viewing volume. Here the SP2 was operated with a sample flow rate of only 60 cm³/min, or half of the typical value, to minimize the

influence of particle coincidence. Inspection of individual particle detection events indicates that particle coincidence was generally avoided by operating at this reduced flow rate.

The SP2 data were processed using the SP2 Toolkit from the Paul Scherer Institute, developed by Martin Gysel. The SP2 was calibrated using size-selected fullerene particles (Lot L20W054, Alfa Aesar, Ward Hill, MA, USA). The SP2 size-dependent counting efficiency was determined by simultaneously measuring the concentration of the calibration particles with a condensation particle counter (TSI, model 3075). The particle counting efficiency was found to be unity for particles with $d_{p,VED} > 100$ nm. The SP2 used in this study measured particles over the size range $76 \text{ nm} \leq d_{p,VED} \leq 822$ nm. Below the lower size limit, the detection efficiency falls off rapidly due, in part, to the large surface area-to-volume (SA-to-V) ratio of these particles. When the SA-to-V ratio is sufficiently large conductive cooling competes effectively with the radiative heating from the laser and the particles do not emit enough incandescent light at short enough wavelengths to trigger detection (Schwarz et al., 2010). Above the upper size limit, the incandescence level is sufficient to saturate the detector, leading to an underestimate of particle mass. All SP2 mass concentration measurements were corrected for the missing mass contained in particles below the lower and above the upper size limit, using a multimode fitting approach (Appendix A).

2.3. Particle Optical Property Measurements

Particle optical properties for PM_{10} were measured at 405 and 532 nm using the UC Davis CRD-PAS at both the Fresno and Fontana sites. Light absorption coefficients (b_{abs} ; units = Mm^{-1}) for dry particles were determined at 405 and 532 nm using photoacoustic spectroscopy (Lack, Langridge, et al., 2012). Light extinction coefficients (b_{ext} ; units = Mm^{-1}) for dry (<20% RH) particles were measured at 405 and 532 nm via CRD spectroscopy (Langridge et al., 2011). Humidified light extinction measurements (RH ~85%) were also measured at 532 nm by CRD spectroscopy. The absorption measurements from the PAS were calibrated relative to the extinction measurement from the CRD using gas-phase O_3 and NO_2 with an estimated accuracy of 5% at 532 nm and 8% at 405 nm.

At the Fresno site optical properties were also measured at 870 nm using a photoacoustic extinctionometer (PAX; DMT, Inc.). In the PAX, light absorption coefficients were measured by photoacoustic spectroscopy. Light-scattering coefficients (b_{scat} ; units = Mm^{-1}) were determined for dry particles with the PAX using reciprocal nephelometry. The absorption measured by the PAX was calibrated relative to the UC Davis PAS using polydisperse fullerene soot and assuming that the AAE was 1.4 (Metcalf et al., 2013), with an estimated uncertainty of 10%.

2.4. Particle Composition Measurements

2.4.1. Composition and Concentration of Nonrefractory Particulate Matter

The concentration of nonrefractory particulate matter (NR-PM) species in PM_{10} were measured using a high-resolution time-of-flight aerosol mass spectrometer (HR-ToF-AMS, henceforth HR-AMS; Canagaratna et al., 2007) during both the Fresno and Fontana studies, as discussed in detail by Chen et al. (2018). The NR-PM components are functionally defined as those materials that evaporate rapidly after impaction onto a heated surface in vacuo at ~600 °C. The NR-PM components characterized include particulate sulfate, nitrate, ammonium, chloride, and organic matter. The data were processed using the PIKA toolkit in IGOR (Wavemetrics, Inc.). The OA composition data were further analyzed using positive matrix factorization (PMF; Zhang, Jimenez, et al., 2011). Four OA factors were determined during the Fresno campaign, identified as biomass burning OA (BBOA), hydrocarbon-like OA (HOA), and two types of oxygenated OA identified as a very oxygenated OA (VOOA) type and a nitrate-associated OA (NOOA) type (Chen et al., 2018). For Fontana, four OA factors were also determined and identified as hydrocarbon-like OA (HOA), cooking-related OA (COA), and two oxygenated OA factors, referred to here as a more-oxidized very oxidized OA (VOOA) and a less-oxidized, NOOA type (Chen et al., 2018). (The particular terminology used here for the OA factors is discussed in Chen et al., 2018.)

2.4.2. Composition and Concentration of BC-Containing Particles

The concentrations and composition of only BC-containing particles were determined using a SP-AMS (Onasch et al., 2012), for both the Fresno site (Collier et al., 2018) and the Fontana site (Lee et al., 2017). In the SP-AMS, a focused particle beam is intersected with an intracavity Nd:YAG laser operating at 1,064 nm. Particles containing BC are rapidly heated by the laser, leading to evaporation of both the

NR-PM materials and the refractory BC. In these studies, the standard HR-AMS tungsten vaporizer was removed so that particles that do not contain BC are not vaporized and are therefore not detected. Thus, the SP-AMS is specific to BC-containing particles, as operated here. In addition to BC, the SP-AMS measures the internally mixed particulate inorganic (sulfate, nitrate, ammonium, and chloride) and organic mass loading. The NR-PM species that are associated with BC will be distinguished from the bulk average NR-PM species (from the HR-AMS) using the subscript BC (i.e., NR-PM_{BC}). The SP-AMS particle detection efficiency is determined in large part by the extent of overlap between the particle and laser beam. Particles were sampled through a PM₁ aerodynamic lens, with particles measured down to ~40-nm vacuum aerodynamic diameter. For the Fresno data set, the detection efficiency was determined by referencing the BC concentration measured by the SP-AMS to that measured by the SP2 (Collier et al., 2018). The SP-AMS/SP2 ratio was observed to depend on the ratio between the NR-PM_{BC} and BC, with the NR-PM/BC ratio increasing as the SP-AMS/SP2 ratio increases, similar to previous observations (Willis et al., 2014). This is likely a result of the BC-containing particles becoming more spherical as NR-PM coatings accumulate. This leads to greater collimation of the particle beam, better overlap with the laser, and ultimately an increased detection efficiency. The dependence of the detection efficiency on the NR-PM/BC ratio was empirically determined for the Fresno study and has a functional form similar to that previously reported for laboratory studies (Willis et al., 2014). For the Fontana data set, the SP-AMS collection efficiency was estimated based on measurements of the particle beam width, and a single, average value was used (Lee et al., 2017). At the Fontana site, the SP-AMS was operated alternating between ensemble mode (i.e., bulk composition) and event-trigger mode (single-particle composition), and the observations were analyzed using PMF (Lee et al., 2017). The coating-to-core mass ratio for both campaigns is calculated directly from the SP-AMS measurements as $R_{\text{coat-rBC}} = [\text{NR-PM}]_{\text{BC}}/[\text{BC}]$.

2.5. Other Instrumentation

Number-weighted particle size distribution measurements for ambient and thermodenuded particles were made using a SEMS (Brechtel Manufacturing, Inc.), operating over the mobility diameter size range 10–950 nm. The SEMS consisted of a differential mobility analyzer and a mixing condensation particle counter.

2.6. Determination of Intensive Particle Properties

The light absorption coefficient and BC concentration measurements are used to determine the observed mass absorption coefficient, referenced to BC, as

$$\text{MAC}_{\text{BC}} = \frac{b_{\text{abs}}}{[\text{BC}]}; \quad (1)$$

The observed MAC_{BC} may include contributions to absorption from non-BC components (e.g., BrC), whether internally or externally mixed, or from nonabsorbing coatings via the lensing effect. The observable absorption enhancement can be determined from the MAC_{BC} values by normalizing MAC_{BC} by a reference value for pure, uncoated BC, with

$$E_{\text{abs}} = \frac{\text{MAC}_{\text{BC}}}{\text{MAC}_{\text{BC,ref}}}; \quad (2)$$

The reference $\text{MAC}_{\text{BC,ref}}$ can be established from the literature (Bond & Bergstrom, 2006) or from the observations by extrapolating MAC_{BC} to the limit of $R_{\text{coat-rBC}} = 0$; the latter approach is taken here (discussed further in section 3.3), although both methods give similar results for the current campaigns. The absorption enhancement can also be determined from simultaneous or sequential measurements of b_{abs} for ambient particles and thermodenuded particles (Cappa et al., 2012; Healy et al., 2015; Liu, Aiken, et al., 2015). As noted above, sequential b_{abs} measurements of ambient and thermodenuded particles were made on a 5-min cycle. In the current study, we focus on E_{abs} as determined from equation (2) above. The E_{abs} from equation (2) (i.e., from the *MAC-method*) are compared to E_{abs} determined from the *thermodenuder-method* in Appendix B.

The wavelength dependence of the absorption coefficient is characterized by the AAE as

$$AAE = -\log\left(\frac{b_{\text{abs},\lambda_1}}{b_{\text{abs},\lambda_2}}\right) / \log\left(\frac{\lambda_1}{\lambda_2}\right); \quad (3)$$

where λ_1 and λ_2 indicate two different measurement wavelengths. The wavelength dependence of the imaginary refractive index, k , can alternatively be characterized by the parameter w , where

$$w = -\log\left(\frac{k_{\lambda_1}}{k_{\lambda_2}}\right) / \log\left(\frac{\lambda_1}{\lambda_2}\right) \quad (4)$$

The AAE and w can be determined from wavelength pairs or from fitting multiwavelength data.

3. Results and Discussion

3.1. General Overview

Chen et al. (2018) provide a broad overview of the campaigns, and Lee et al. (2017) and Collier et al. (2018) provide details on the SP-AMS measurements specifically. Here we highlight a few details from each campaign that are relevant to the current study. Time series of light extinction and light absorption for the two campaigns are shown in Figure 2 for reference.

The wintertime Fresno campaign is separated into two distinct time periods based on the local meteorology. In particular, after about 6 January, 2015, the morning was impacted by a persistent, relatively thick fog that would slowly dissipate as the day progressed. Prior to this date, the atmosphere is classified as being substantially less foggy. The heavy fog period will be referred to as *high* fog and the less foggy period as *low* fog. The low-fog period was colder and drier than the high-fog period ($T_{\text{avg}} = 7.6$ °C and $\text{RH}_{\text{avg}} = 80.7\%$ versus $T_{\text{avg}} = 12.0$ °C and $\text{RH}_{\text{avg}} = 83.5\%$). The diurnal variability and average particle composition and concentrations were distinct between the low-fog and high-fog periods (Chen et al., 2018), and a clear increase in extinction was observed in the high-fog period; the average $b_{\text{ext},532\text{nm}}$ during the low-fog period was 73 Mm^{-1} and 226 Mm^{-1} during the high-fog period. The average BC coating amount was also larger during the high-fog period than the low-fog period, with $R_{\text{coat-rBC}}$ (low fog) = 2.1 ± 0.8 versus $R_{\text{coat-rBC}}$ (high fog) = 2.8 ± 0.4 (Collier et al., 2018). The diurnal variation in $R_{\text{coat-rBC}}$ was more pronounced during the low-fog period than the high-fog period, with the daytime values being slightly elevated over nighttime values (Collier et al., 2018). The daytime $R_{\text{coat-rBC}}$ values during the low- and high-fog periods were similar. Thus, much of this increase was attributable to a substantial increase in the particulate NO_3^- during the high-fog period, although the OA was also larger during the high-fog period (Chen et al., 2018). Of particular relevance to the current study, the fraction of organics classified as BBOA was larger during the low-fog period, while the NOOA contribution increased substantially during the high-fog period. There was substantially greater diurnal variability in the absorption and extinction during the low-fog period than during the high-fog period.

The Fontana campaign was characterized by generally high temperatures ($T_{\text{avg}} = 23.6$ °C; range 14.9 to 35.9 °C) and relatively low RH ($\text{RH}_{\text{avg}} = 55\%$), with strong diurnal variability in both (Chen et al., 2018). Early in the campaign, the atmosphere was strongly impacted by fireworks associated with the 4 July (U.S. Independence Day) activities; the impact of the 4 July activities persisted through 8 July. This fireworks-impacted period is separated for analysis from the remaining nonfireworks days. The average $b_{\text{ext},532\text{nm}} = 30 \text{ Mm}^{-1}$ for the nonfireworks impacted period. The diurnal profile of NR-PM has two peaks, one at 10:00 and another at 17:00 (local times; Chen et al., 2018). The mean $R_{\text{coat-rBC}}$ was much larger than in Fresno, with $R_{\text{coat-rBC,avg}} = 5.2$, and the diurnal variation in $R_{\text{coat-rBC}}$ is large, with a single maximum at 16:00 (Lee et al., 2017).

3.2. BC Concentrations and Size Distribution

The average mass-weighted BC-only size distributions, determined from multimodal fitting of the observed SP2 measurements for each campaign, are shown in Figure 2. For each campaign, the BC-only size distributions exhibit multimodal character. For example, Fresno exhibited dominant mode maxima between $d_{p,\text{VED}} \sim 45\text{--}60$ nm and at 115–160 nm (Figure 3), consistent with previous measurements in this region (Zhang et al., 2016). Figure 3 shows mass-weighted size distributions determined from multimodal fitting of the

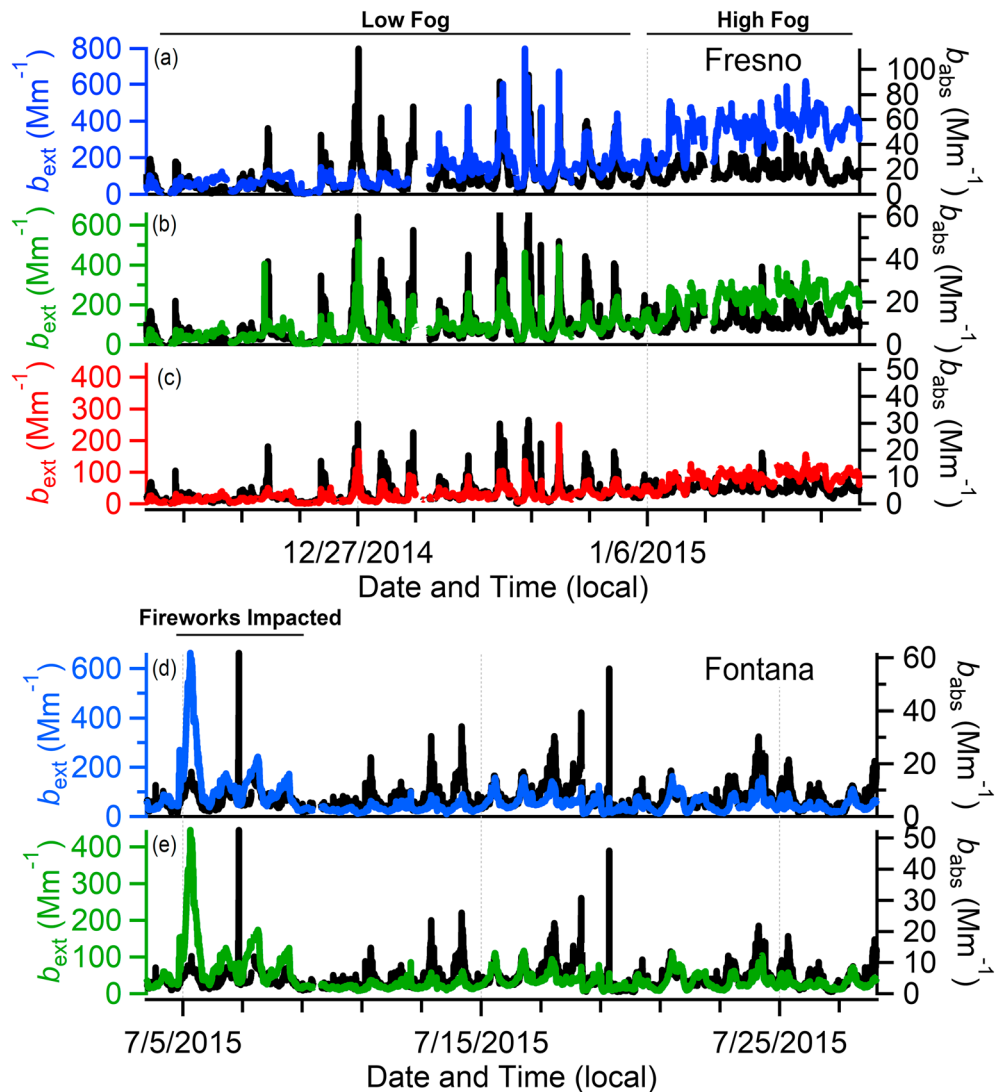


Figure 2. Time series of particle light extinction (left axes, color) or absorption (right axes, black) for (a–c) Fresno and (d–e) Fontana at (a and d) 405 nm, (b and e) 532 nm, and (c) 870 nm.

observed size distributions. Details of the fitting procedure used to determine the mass-weighted BC size distribution over the entire size range and the associated uncertainties are discussed in Appendix A.

Fresno: The multimode fits indicate that on average $31_{-7}^{+13}\%$ of the BC mass is outside of the detection range of the SP2 used here, with a larger amount of missing mass during daytime than at nighttime. The relative contribution of the larger mode is greater at night, with the smaller mode more pronounced during the day. The greater contribution of particles with larger volume equivalent BC core diameters during nighttime reflects an increased concentration of biomass-combustion derived BC particles, as biomass-burning-derived BC particles have larger diameters than fossil fuel-derived particles (in particular, those from vehicular emissions; Kondo et al., 2011). Consideration of the diurnal variability of the BC concentrations in each of the four fit modes (Appendix A) demonstrates that the smallest two modes (at 57 and 118 nm) exhibit a sharp increase starting at 06:00 (Figure 3b), reflecting substantial BC emissions during the morning rush hour coupled with the still relatively low boundary layer height. The larger two modes (at 182 and 420 nm) increase primarily at night, when residential wood combustion is largest and the nocturnal boundary layer is shallow. The BC concentration in the two small modes also increases at night, primarily a reflection of the decreased boundary layer height relative to daytime along with continued emissions, although

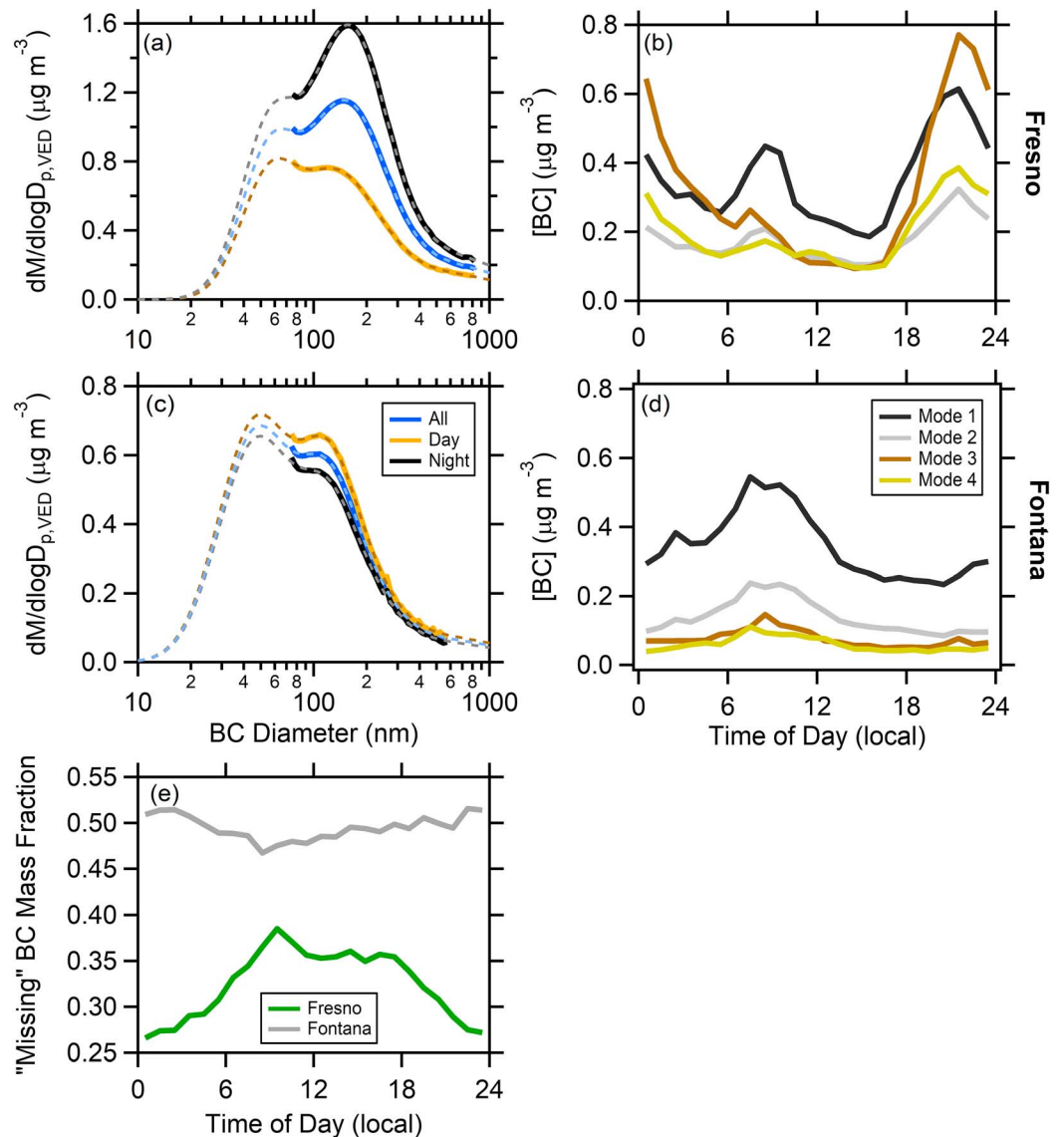


Figure 3. (a and c) Observed mass-weighted black carbon (BC)-specific size distributions (solid lines) and multi-mode fits (dashed lines) for (a) Fresno and (c) Fontana. The blue lines are for all periods, the orange for daytime, and the black for nighttime. (b and d) The diurnal variation in the BC mass concentration of each of the four modes fit to the mass-weighted distributions. The mode diameter increases with the mode number. Mode diameters are reported in section 3.2. (e) The diurnal variability in the estimated BC missing-mass fraction, calculated from the difference between the fit distributions and observed distributions, for Fresno (green) and Fontana (gray).

their fractional contribution is decreased. However, the peak concentration in these modes occurs ~ 1 hr earlier in the night than of the larger two modes, reflecting the different sources. The campaign-average fractional contribution of the vehicle-related modes (the two smallest) was $0.5^{+0.10}_{-0.07}$, meaning half the BC came from vehicles and half from biomass burning, with the limitation that the modes may not be purely reflective of one source or the other (i.e., there may be some small particles contributed by biomass combustion and some larger particles from vehicles). These observations demonstrate that there are two distinct sources of BC in the wintertime Fresno atmosphere, one from motor vehicles (likely, diesel vehicles) and one from biomass combustion.

Fontana: For Fontana, the BC-only mass-weighted size distributions also had multiple modes. However, at this site the smallest two modes (at 47 and 116 nm) contributed the majority of the BC mass, with their

campaign-average fractional contribution being $0.78_{-0.1}^{+0.16}$. This indicates that vehicle emissions dominate the BC burden in the region. The small contribution from the two larger modes (at 182 and 420 nm) could indicate some contribution from regional biomass burning. Alternatively, these larger particles could result from near-source coagulation and could also be contributed by motor vehicle emissions. The contribution from the larger modes was enhanced from the night of 4 July through the following night, indicating that fireworks (from the 4 July celebrations) produced BC having larger diameters. Overall, $53_{-12}^{+22}\%$ of the BC mass was contained in particles outside of the SP2 detection range, with minimal diurnal variability (and most of the variability in the campaign-average resulting from the enhanced large particle contribution on 4 July).

3.3. Variability in MAC_{BC} and E_{abs}

3.3.1. Determination of Reference BC Mass Absorption Coefficients

The total observed absorption, and the associated MAC_{BC} , results from a combination of absorption by BC, including mixing-induced enhancements, and absorption by BrC. The diurnal variation in the observed MAC_{BC} values for both campaigns and histograms of MAC_{BC} are shown in Figure 4. For Fresno, the MAC_{BC} distribution at 405 nm is quite broad and exhibits a clear increase at night and again during the day, with minima at 09:00 and 17:00 (local time). The MAC_{BC} values at 532 and 870 nm exhibit similar, but much less pronounced, diurnal variability, and the spread of the MAC_{BC} distributions decreases substantially with wavelength. The diurnal variability of MAC_{BC} attributable to mixing-induced enhancements alone should exhibit a negligible wavelength dependence. Thus, the observed wavelength-dependent behavior indicates that diurnal-varying BrC contributes substantially to the observed MAC_{BC} . In Fresno, the diurnal variability differed substantially between the low-fog and high-fog periods at 405 nm in particular, but also at 532 nm. During the low-fog period, the daytime MAC_{BC} increase was suppressed, while during the high-fog period, it was enhanced (relative to the campaign average).

In Fontana, the MAC_{BC} values at 405 and 532 nm, excluding the fireworks-impacted period, increased during the early morning and stayed elevated through the afternoon (Figure 4). But, the overall day-night difference was much smaller compared to that observed in Fresno, and the MAC_{BC} distributions were also narrower than in Fresno. (When periods impacted by fireworks are included, the MAC_{BC} in the early morning [−06:00] is increased because the MAC_{BC} during the fireworks-impacted period was particularly large at this time.)

The observed MAC_{BC} values can be converted to equivalent absorption enhancement values by dividing by a reference MAC for pure, uncoated BC (referred to here as $MAC_{BC,ref}$). While values of the $MAC_{BC,ref}$ are reported in the literature, quantitative comparison to the ambient observations can be challenged by the uncertainty in the BC concentration measurement, in particular. This is especially the case here, given the large, time-varying *missing mass* correction required. Thus, a wavelength-specific reference $MAC_{BC,ref}$ for uncoated BC has been determined for each campaign from the observations. Estimation of campaign-specific $MAC_{BC,ref}$ in this manner allows for more robust determination of E_{abs} than if the literature values were used, accounting for any campaign-specific sampling biases. However, this method does not account for potential changes in the $MAC_{BC,ref}$ that result from changes in morphology that can result from coating of materials onto BC.

Ideally, the reference $MAC_{BC,ref}$ can be determined by extrapolating the observed MAC_{BC} measured for either ambient particles or particles passed through the thermodenuder to the limit of no coating material (i.e., as $R_{coat-rBC} \rightarrow 0$). For Fresno this method is complicated by two factors: (i) the cooccurrence of BrC that is likely externally mixed from the BC and (ii) the potential charring of the NOOA (see Appendix B). There is, however, a reasonable relationship between $R_{coat-rBC}$ and both the overall $[OA]/[rBC]$ and $[NR-PM_1]/[rBC]$ ratios (Figure S3). Thus, it is reasonable to extrapolate the observed ambient particle MAC_{BC} to the limit of $[OA]/[rBC] = 0$, as this reflects a condition where there is concurrently little coating material and little externally mixed absorbing OA. The Fresno observations at all three wavelengths are consistent with a sigmoidal relationship between MAC_{BC} and $[OA]/[rBC]$ for Fresno (Figure S4). The resulting campaign-specific $MAC_{BC,ref}$ values for Fresno are 4.4 ± 0.2 m²/g (870 nm), 7.5 ± 0.5 m²/g (532 nm), and 10.7 ± 0.6 m²/g (405 nm), where the reported uncertainties correspond to the 99% confidence interval from the fit. The distributions of observed MAC_{BC} values are compared to the derived $MAC_{BC,ref}$ values in Figure S5. For Fontana, this method of estimation is complicated by the particles sampled during the fireworks

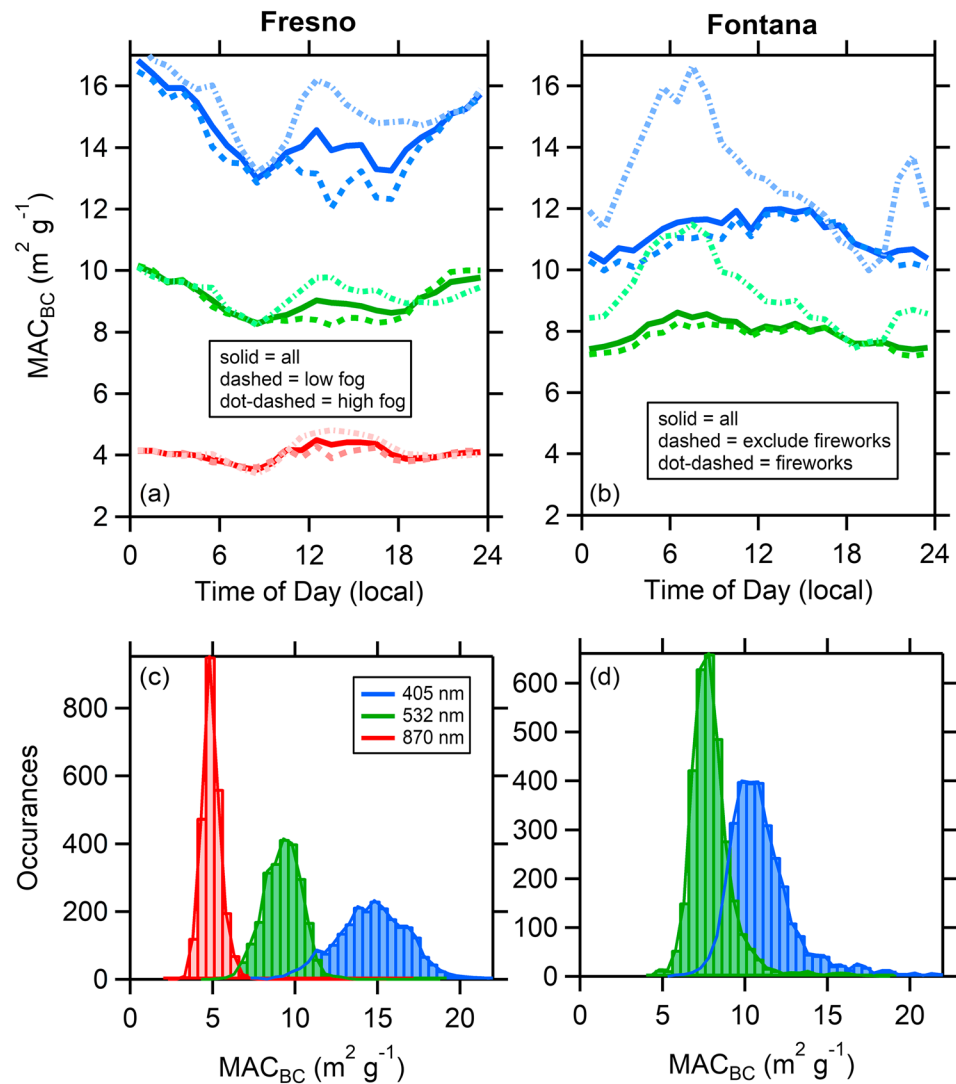


Figure 4. Observed diurnal variation in the black carbon (BC) mass absorption coefficients (MAC_{BC}) in (a) wintertime Fresno and (b) summertime Fontana. For both campaigns the solid lines are the all-campaign averages. For Fresno, the dashed line is for the low-fog period and the dot-dashed is for the high-fog period. For Fontana, the dashed line excludes the period impacted by fireworks (i.e., around the 4 July) and the dot-dashed line is for the fireworks-impacted period. Histograms of the observed MAC_{BC} values for (c) Fresno and (d) Fontana.

period, which were particularly nonvolatile and, likely, subject to charring. Therefore, only observations of MAC_{BC} and $R_{coat-rBC}$ outside of the fireworks-impacted period are used to determine the $MAC_{BC,ref}$ (Figure S6). The campaign-specific values for Fontana are $7.2 \pm 0.1 \text{ m}^2/\text{g}$ (532 nm) and $9.6 \pm 0.2 \text{ m}^2/\text{g}$ (405 nm) where the reported uncertainties correspond to the 99% confidence interval from the fit. The distributions of observed MAC_{BC} values are compared to the derived $MAC_{BC,ref}$ values in Figure S7. The absolute uncertainty on these $MAC_{BC,ref}$ values is large given the relatively large uncertainty on the SP2 measurements, and the fit-based uncertainties for the Fontana measurements are smaller than is reasonable. We suggest that a reasonable precision-limited uncertainty on the $MAC_{BC,ref}$ values for both campaigns is 10%. It is noteworthy that the derived campaign-specific $MAC_{BC,ref}$ values are in reasonable agreement with laboratory measurements (Cross et al., 2010; Forestieri et al., 2018) and literature assessments (Bond & Bergstrom, 2006). They are, however, substantially smaller than recently determined from filter-based measurements made across Europe for ambient particles, where the MAC at 637 nm was reported as $10.0 \text{ m}^2/\text{g}$, which would correspond to an MAC at 532 nm of $12 \text{ m}^2/\text{g}$ assuming an AAE = 1.

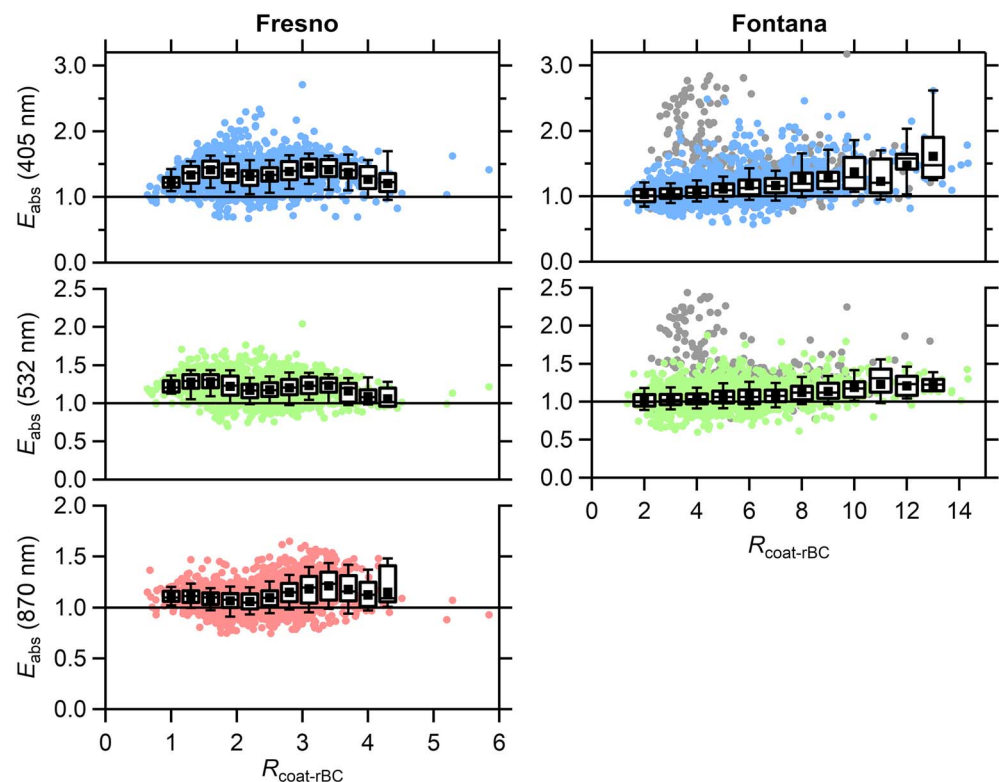


Figure 5. The dependence of the absorption enhancement (E_{abs}) on the black carbon (BC) coating-to-core mass ratio ($R_{\text{coat-rBC}}$) for 405 nm (blue, top), 532 nm (green, middle), and 870 nm (red, bottom). Results are shown separately for (left) Fresno and (right) Fontana. The points are the individual 10-min averages, colored according to wavelength. The box and whisker plots show the mean (■), median (—), lower and upper quartile (boxes), and 9th and 91st percentiles (whisker). For Fontana, the gray points indicate the fireworks-impacted period, which are not included in the box and whisker plots.

3.3.2. Absorption Enhancement: Observations

The E_{abs} values derived from the MAC_{BC} observations are shown as a function of the BC coating amount ($R_{\text{coat-rBC}}$) in Figure 5. In Fresno, the E_{abs} values at 405 and 532 nm are notably greater than unity for all $R_{\text{coat-rBC}}$ (from 1 to 4). The mean values are 1.37 ± 0.22 (405 nm), 1.22 ± 0.15 (532 nm), and 1.10 ± 0.13 (870 nm). In contrast, the E_{abs} in Fontana are very close to one when $R_{\text{coat-rBC}}$ is in this same range, with $E_{\text{abs}} = 1.10 \pm 0.27$ (405 nm) and 1.07 ± 0.22 (532 nm), excluding the fireworks-impacted period. There is, however, a small, increase in E_{abs} with $R_{\text{coat-rBC}}$ in Fontana. E_{abs} values binned by $R_{\text{coat-rBC}}$ are also shown in Figure 1 for Fresno (at 781 nm) and Fontana (at 532 nm) with the literature observations.

The differences in the dependence of E_{abs} on $R_{\text{coat-rBC}}$ between Fresno and Fontana result primarily from differences in the contribution of BrC to the total absorption between the two locations. Chen et al. (2018) determined four general types of OA based on PMF analysis of the HR-AMS data for both sites. In Fresno, there is a substantial contribution of BrC from biomass burning that enhances the E_{abs} above unity even at low $R_{\text{coat-rBC}}$. The fractional contribution from the biomass-burning associated factor (BBOA) is largest when $R_{\text{coat-rBC}}$ is smallest (Figure 6). Consistent with this, the fractional contribution of the $\text{C}_2\text{H}_4\text{O}_2^+$ ion (an AMS marker for biomass burning) in the BC coating material is higher when $R_{\text{coat-rBC}}$ is smallest (Collier et al., 2018). This suggests that absorption by BBOA, whether internally or externally mixed from BC, contributes importantly to the $E_{\text{abs}} > 1$ at low $R_{\text{coat-rBC}}$ for Fresno. The fractional contribution of the NOOA increases as $R_{\text{coat-rBC}}$ increases. This suggests that the NOOA might be somewhat absorbing and contributes to the $E_{\text{abs}} > 1$ at larger $R_{\text{coat-rBC}}$, especially at 405 nm. For Fontana, four OA factors were also identified. There, the OA mass is dominated by the VOOA factor, and the fractional contribution of VOOA increases with $R_{\text{coat-rBC}}$ (Figure 6). Some of the increase in E_{abs} with $R_{\text{coat-rBC}}$ for Fontana might therefore result from photochemical production

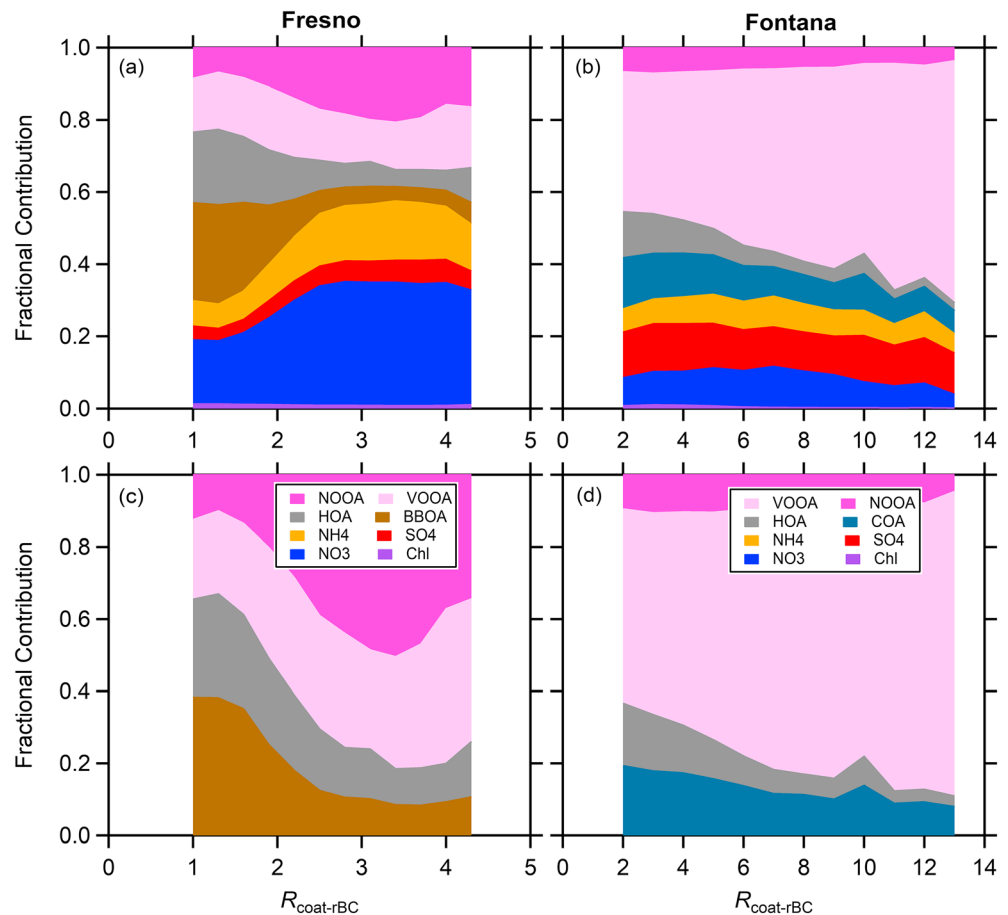


Figure 6. The variation of the fractional contribution of all nonrefractory particulate matter species (both internally and externally mixed with black carbon [BC]) versus $R_{\text{coat-rBC}}$ for (a) Fresno and (b) Fontana. The variation in only the organic aerosol factors with $R_{\text{coat-rBC}}$ for (c) Fresno and (d) Fontana.

of coatings on BC. Further discussion of absorption by OA follows below. Regardless of the exact reason for the increase in E_{abs} with $R_{\text{coat-rBC}}$ at Fontana, comparison with the theoretical calculations in Cappa et al. (2012) or Liu, Aiken, et al. (2015) demonstrates that the magnitude of the E_{abs} observed in Fontana is much lower than might be expected from simple application of core-shell Mie theory.

3.3.3. Absorption Enhancement: Interpretation

The small E_{abs} values in Fontana at both 405 and 532 nm, even at high $R_{\text{coat-rBC}}$ (~10), are consistent with the observations of Cappa et al. (2012), who similarly observed small E_{abs} values (<1.1) at high $R_{\text{coat-rBC}}$. A large fraction of the Cappa et al. (2012) measurements were made in the coastal waters around Los Angeles, CA, while the Fontana measurements here were made in the inland greater LA area. In contrast, Liu, Aiken, et al. (2015), using similar methods, observed mean E_{abs} values at 781 nm of ~1.5 at moderate $R_{\text{coat-rBC}}$ (~4) in a somewhat rural area located near London, UK. The assumption for the core-shell Mie theory calculations in those studies was that the coating material is equally distributed across the particle population. Under this assumption, there is an expectation that the ensemble-average E_{abs} from mixing effects (i.e., lensing) should increase with the ensemble-average $R_{\text{coat-rBC}}$, just as it does for individual particles (Bond et al., 2006; Fuller et al., 1999). It is evident that the observed dependence of E_{abs} on $R_{\text{coat-rBC}}$ does not consistently follow this model and certainly does not for the CA observations. This likely results from there being different populations of BC-containing particles having varying coating amounts, with some particles having *thick* coatings and others having *thin* coatings as indicated from PMF analysis of the Fontana SP-AMS observations (Lee et al., 2017). Fierce et al. (2016) argue from a model perspective that accounting for particle diversity and

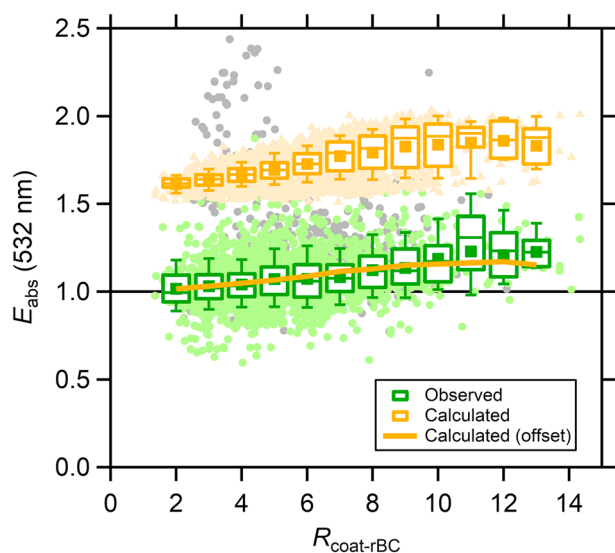


Figure 7. Comparison between the observed (green) and calculated (orange) E_{abs} versus $R_{\text{coat-rBC}}$ relationship for 532 nm at Fontana. The solid orange line is the mean calculated value, multiplied by 0.65. The points are the individual 10-min averages; the gray points show the fireworks-impacted period. The box and whisker plots show the mean (■), median (—), lower and upper quartile (boxes), and 9th and 91st percentiles (whisker) for the nonfireworks-impacted data.

the actual distribution of coating material can have a strong impact on the population-averaged absorption, typically leading to a decrease in absorption compared to the equivalent uniformly coated population and therefore a smaller E_{abs} . Liu et al. (2017) provide experimental evidence in line with this conclusion. This suggests that the observation of small E_{abs} values here and in Cappa et al. (2012) at relatively high $R_{\text{coat-rBC}}$ is likely a result of mixing state (and coating amount) diversity within the BC particle population. However, we cannot rule out the possibility that morphological deviations (i.e., the distribution of coatings and BC within individual particles) from the ideal core-shell morphology also contribute to a reduced ensemble-average E_{abs} .

The SP-AMS PMF results from Lee et al. (2017) for Fontana specifically indicated four BC-containing types of particles having different BC weight percentages. These were identified by PMF as an HOA-rich factor (14.2%), a BC-rich factor (44.4%), and two oxygenated factors, termed OOA-1 (13.4%) and OOA-2 (0.5%), where the numbers in parentheses are the factor-specific BC wt%. The fractional contribution of the OOA-1 factor increased with $R_{\text{coat-rBC}}$ while the BC-rich and, to a lesser extent, the HOA-rich factor contributions decreased (cf. Figure 4 in Lee et al., 2017). The OOA-2 factor contributed a large proportion of the overall coating material mass but contained little of the BC. Assuming core-shell morphologies for each factor, the factor-specific E_{abs} can be calculated from Mie theory. The calculated factor-specific E_{abs} are 1.45 (BC-rich), 2.05 (HOA-rich), 1.99 (OOA-1), and 2.43 (OOA-2) at 532 nm, assuming a

core BC diameter of 120 nm (one of the mode diameters for Fontana) and accounting for density differences between BC and the coating material. The ensemble-average E_{abs} can be calculated using a linear combination of these four factors with the fraction types from Lee et al. (2017). The calculated ensemble-average E_{abs} is greater than the observed E_{abs} at all $R_{\text{coat-rBC}}$ (Figure 7). This is not surprising given that the smallest factor-specific E_{abs} (for the BC-rich type) was larger than the observed ensemble-average even at large $R_{\text{coat-rBC}}$

However, the dependence of the observed and calculated ensemble-average E_{abs} and $R_{\text{coat-rBC}}$ are similar if the calculated ensemble-average E_{abs} is multiplied by 0.65 (Figure 7). This, perhaps, indicates that changes in the fractional contribution of the different BC-containing particle factors with $R_{\text{coat-rBC}}$ are responsible for the slow increase in E_{abs} with $R_{\text{coat-rBC}}$, but that the calculated E_{abs} based on the average properties of each BC-containing factor are nonetheless overestimated when core-shell Mie theory is used. This could indicate additional particle-to-particle (or size-dependent) diversity in the coating amount even within each identified factor (Fierce et al., 2016) or could result from particles having non-core-shell morphologies that limit the extent of the absorption enhancement (Adachi et al., 2010; Scarnato et al., 2013). Regarding the role of particle-to-particle diversity, Fierce et al. (2016) calculated that the absorption enhancement for their particle resolved ensemble was 1.3 whereas had they assumed uniform coating across the population the absorption enhancement was 2.3. Regarding the potential for non-core-shell morphologies to explain the results, Scarnato et al. (2013) calculate using a discrete dipole approximation model MAC values for BC having no coating, BC being only partially immersed in a coating, and for BC being completely immersed. The MAC values they calculated for partially immersed BC are negligibly different than that for the bare BC, whereas the MAC for the completely immersed BC is a factor of 1.5–1.7 times larger, with the range indicating slight differences between lacy BC and compact BC aggregates. Both studies are thus consistent both qualitatively and quantitatively with the empirical scaling factor determined here. Most likely, both phenomena contribute. The inability of even the factor-specific core-shell E_{abs} calculations to reproduce the observations suggests that the core-shell approach may not be wholly appropriate for use in climate models, especially when they do not account for particle population diversity.

Regardless, the question persists as to the reason why the $E_{\text{abs}}-R_{\text{coat-rBC}}$ relationship seemingly differs between the urban and near-urban CA atmosphere and the UK atmosphere. We hypothesize that this difference is linked to the sources and age of the air masses sampled. In Liu, Aiken, et al. (2015) the

largest $R_{\text{coat-rBC}}$ values were observed to have particularly large BC core diameters, suggesting a biomass-burning source. However, these same particles also had the largest fraction of oxygenated OA, suggestive of photochemical or even cloud processing, and back trajectory analysis indicated that when $R_{\text{coat-rBC}}$ was large the sampled air masses tended to come from the European continent, while air masses tended to come from within the UK when $R_{\text{coat-rBC}}$ was small. It may be that longer-range transport serves to decrease the differences in coating amounts between the different BC-containing particle types observed in nearer-source regions and periods (Lee et al., 2015; Lee et al., 2017) and thus increases the consistency between simple core-shell calculations and observations of ensemble-average absorption. However, in Toronto, Canada, Healy et al. (2015) did not observe an increase in E_{abs} for periods identified as being impacted by transboundary (i.e., long-range) pollution, even though the $R_{\text{coat-rBC}}$ was ~ 3.5 during this period. It is possible that their observations were confounded by inputs from local BC sources that served to maintain the particle-to-particle diversity (with respect to coating amount) and limit the overall observed E_{abs} . The results presented here indicate that measurements in remote locations that are reasonably free from local inputs (whether anthropogenic, such as from vehicles, or from fresh biomass burning) would be helpful in understanding the extent to which E_{abs} changes as a result of atmospheric processing. However, such measurements will be challenged by the low signals and BC concentrations that are typically observed in remote regions. It is suggested that a minimum of 1 month of measurements will be required to build sufficient statistics in low-concentration locations.

3.4. BrC Absorption

3.4.1. Methodology

To assess the contribution of BrC to the total observed absorption requires removal of the contribution from the mixing-induced enhancement, that is, the lensing effect. Here we take two approaches. In the first, an upper limit for the contribution of BrC to total absorption is determined by assuming that the mixing-induced enhancement is unity. In the second, we estimate the $R_{\text{coat-rBC}}$ -dependent magnitude of the mixing-induced enhancement for each site based on the longest wavelength measurement available (870 nm for Fresno and 532 nm for Fontana), assuming that BrC contributes negligibly at this wavelength. For Fontana this assumption is questionable since some BrC is known to absorb at 532 nm. However, in the absence of longer wavelength measurements this assumption allows us to place a lower bound on the absorption by BrC. The absorption from BrC is then calculated as the difference between the observed absorption and the estimated absorption by coated BC (i.e., inclusive of the mixing-induced enhancement). More specifically,

$$b_{\text{abs,BrC}} = b_{\text{abs,obs}} - b_{\text{abs,BC,coated}} = b_{\text{abs,obs}} - \text{MAC}_{\text{BC,ref}} \cdot E_{\text{abs,mixing}}(R_{\text{coat-rBC}}) \cdot [\text{rBC}] \quad (5)$$

where $b_{\text{abs,BrC}}$, $b_{\text{abs,obs}}$, and $b_{\text{abs,BC,coated}}$ are the absorption by BrC, the observed absorption, and the estimated absorption for coated BC particles, respectively. The $\text{MAC}_{\text{BC,ref}}$ values are those determined above. For the first (upper limit) approach, $E_{\text{abs,mixing}} = 1$. For the second approach the $E_{\text{abs,mixing}}$ values are a function of $R_{\text{coat-rBC}}$ and estimated from the longest-wavelength measurements. Note that equation (5) provides for internal consistency because the $\text{MAC}_{\text{BC,ref}}$ values are determined directly from the observations and are not from the literature; that is, they are campaign-appropriate and account for uncertainties in [BC]. Also, the use of the observationally derived $\text{MAC}_{\text{BC,ref}}$ decreases the sensitivity of the derived $b_{\text{abs,BrC}}$ to uncertainty in the [rBC] because an overestimate in [rBC] would be associated with a corresponding underestimate in the $\text{MAC}_{\text{BC,ref}}$.

As discussed above, the observed $E_{\text{abs}}-R_{\text{coat-rBC}}$ relationship does not follow core-shell Mie theory predictions. Thus, there is no a priori functional form that can be assumed to relate the ensemble average E_{abs} to $R_{\text{coat-rBC}}$ for the second method. We therefore adopt the approach of assuming that the E_{abs} from mixing increases linearly with $R_{\text{coat-rBC}}$, a functional form that is generally consistent with the longest-wavelength observations at each site (870 nm at Fresno and 532 nm at Fontana in Figure 5). However, for the 870-nm measurements in Fresno the observed E_{abs} actually decreases slightly as the $R_{\text{coat-rBC}}$ increases from 1 to ~ 2.5 . We hypothesize that this is indicative of some small absorption by BBOA at 870 nm because the concentration of BBOA decreases as $R_{\text{coat-rBC}}$ increases (discussed later) and is relatively small above $R_{\text{coat-rBC}} \sim 2.5$. Therefore, for Fresno, the relationship between E_{abs} (from mixing effects) and $R_{\text{coat-rBC}}$ is determined from fitting the binned observations only for $R_{\text{coat-rBC}} > 2.5$. Thus, for Fresno it is assumed that there is no

Table 1

The Determined Mass Absorption Coefficients, Imaginary Refractive Indices, Absorption Ångstrom Exponents, and Wavelength Dependencies for the BBOA and NOOA Factors Determined for Fresno

Wavelength (nm)		Lensing corrected ^a			Upper limit ^b		
		BBOA	NOOA	R^2	BBOA	NOOA	R^2
405	MAC	0.84 (0.3)	0.52 (0.18)	0.78	0.84 (0.3)	0.59 (0.2)	0.73
	k	0.024 (0.01)	0.012 (0.07)		0.024 (0.01)	0.015 (0.08)	
532	MAC	0.45 (0.23)	0.14 (0.07)	0.71	0.45 (0.23)	0.21 (0.1)	0.69
	k	0.018 (0.01)	0.005 (0.003)		0.018 (0.01)	0.0077 (0.005)	
870	MAC	0.085 (0.05)	0.044 ^c	0.24	0.093 (0.05)	0.092 ^c	0.35
	k	0.0068 (0.005)	0.007 ^c		0.0075 (0.005)	0.014 ^c	
405–532	AAE	2.28	4.81		2.28	3.79	
	w	1.20	3.67		1.20	2.76	
405–870	AAE	2.99			2.88	--	
	w	1.76			1.76	--	
532–870	AAE	3.39			3.21	--	
	w	2.07			2.07	--	

Note. The estimated uncertainties are reported in parentheses.

^aThe influence of internal mixing (i.e., lensing) on absorption by black carbon (BC) was removed based on the observed dependence of $MAC_{BC}(870)$ nm on $R_{coat-rBC}$. ^bPotential influence from internal mixing (i.e., lensing). ^cUncertainty on this value makes it indistinguishable from 0.

BrC absorption at 870 nm when $R_{coat-rBC} > 2.5$, but that there may be some BrC absorption at lower $R_{coat-rBC}$. For Fontana, the $E_{abs}-R_{coat-rBC}$ relationship is determined from fitting the 532-nm observations over all $R_{coat-rBC}$ because 870-nm measurements are not available. Thus, for Fontana it is inherently assumed that BrC absorption at 532 nm does not result directly in the increase in E_{abs} with $R_{coat-rBC}$. Unless otherwise specified, results reported below refer to the $b_{abs,BrC}$ determined from the second method, but results from both methods are reported in Table 1.

3.4.2. Fresno BrC

3.4.2.1. Observations

For Fresno, absorption by BrC is unambiguous at 405 and 532 nm, with large $b_{abs,BrC}$ values obtained both at night and during the day. For 870 nm, the situation is less clear although there appears to be some absorption by BrC. Comparison of the diurnal profiles of $b_{abs,BrC}$ and the various OA factors (as well as the inorganic species and BC) qualitatively suggests that BBOA and NOOA are somewhat absorbing (Figure 8). A multilinear regression of $b_{abs,BrC}$ against the OA factors confirms that BBOA and NOOA are, indeed, the major absorbing OA types, with regression coefficients (i.e., slopes) of 0.84 and 0.52 m²/g, respectively, and a total $r^2 = 0.78$. The observed and reconstructed absorption are shown in Figure S8. These correspond to the individual mass absorption coefficients for BBOA and NOOA at 405 nm. Similar multilinear fits for the 532 nm $b_{abs,BrC}$ yield regression coefficients corresponding to $MAC_{BBOA} = 0.45$ m²/g and $MAC_{NOOA} = 0.14$ m²/g (combined $r^2 = 0.71$) and for the 870 nm $b_{abs,BrC}$ yield $MAC_{BBOA} = 0.085$ m²/g and $MAC_{NOOA} = 0.044$ m²/g (combined $r^2 = 0.24$). There was no evidence for appreciable light absorption by the two other OA factors, HOA and VOOA. (Although BBOA and HOA have similar diurnal profiles, there is actually only a moderate correlation between the two, with $r^2 = 0.43$. Thus, they are separable in the multilinear fit.) The appropriateness of the multilinear regression and the conclusion that BBOA and NOOA are both BrC (i.e., are absorbing) is visually demonstrated when (i) $b_{abs,BrC}$ is plotted against [BBOA] during periods when the NOOA fractional contribution is small (Figure 9a) or (ii) $b_{abs,BrC}$ is plotted versus [NOOA] when the BBOA fractional contribution is small (Figure 9b). Visual inspection of graphs of HOA and VOOA versus $b_{abs,BrC}$ (not shown) also confirms that neither of these factors are BrC. The OA-factor specific MAC values are shown as a function of wavelength in Figure 10. For the upper limit (no mixing-induced enhancement) approach the derived OA factor-specific MAC values are only slightly larger than those reported above when the mixing-induced enhancement is accounted for NOOA and are the same for BBOA. This indicates a general robustness of the results (Table 1).

The small r^2 from the multilinear regression for 870 nm is expected given that when subtracting the mixing-induced enhancement it was assumed that the OA was nonabsorbing at 870 nm. However, the BBOA is

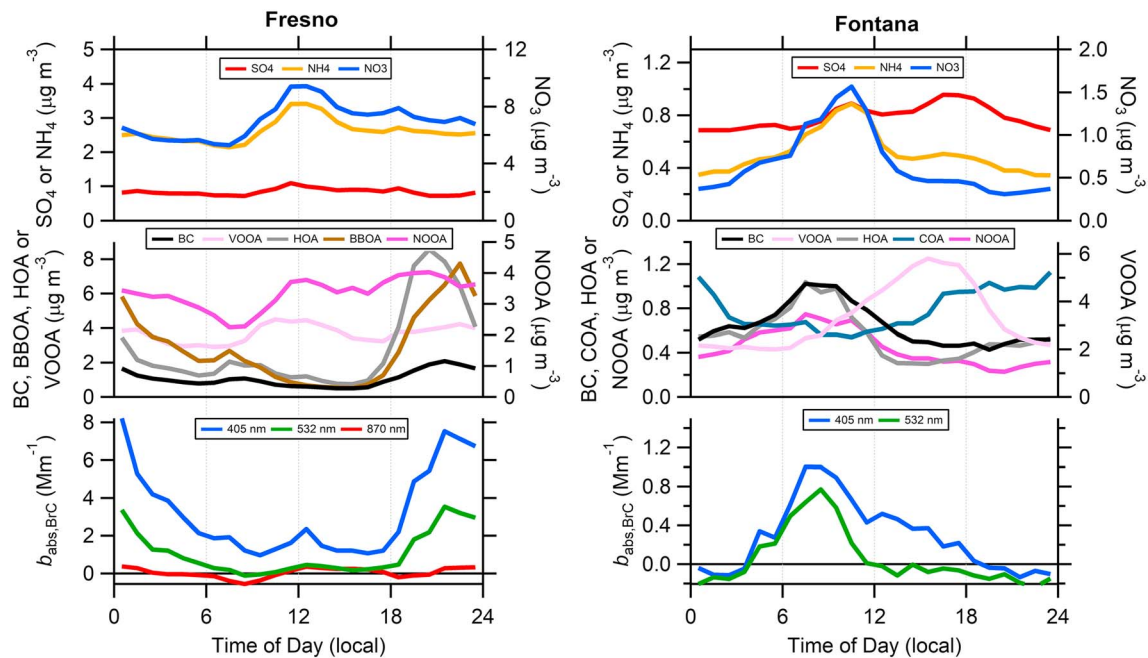


Figure 8. Diurnal variation in the (top panels) inorganic species, (middle panels) brown carbon (BC), and the various organic aerosol factors, and (bottom panels) the absorption attributed to brown carbon, for (left) Fresno and (right) Fontana.

largest when the $R_{\text{coat-rBC}}$ is smallest (where the mixing-induced enhancement is smallest), and thus, there is reason to think that the MAC for BBOA is substantially more reliable than the MAC for NOOA at 870 nm and that the NOOA values at 870 nm might be discounted entirely. This has been tested by performing the multilinear fit for only the low-fog period, when the NOOA concentration was relatively small and the $R_{\text{coat-rBC}}$ was typically <2.5 (the threshold identified above). The retrieved 870 nm $\text{MAC}_{\text{BBOA}} = 0.088 \text{ m}^2/\text{g}$ for the low-fog period, similar to that obtained for the entire data set, and the r^2 was larger ($r^2 = 0.36$).

The uncertainty in these estimates comes from uncertainty in the measurement of [BC], $b_{\text{abs,obs}}$, [BBOA], [NOOA], and the accounting for the mixing-induced enhancement. Since an internally consistent $\text{MAC}_{\text{BC,ref}}$ is used (meaning that this was determined from the observations using the $b_{\text{abs,obs}}$ and [BC]) uncertainty in this value does not contribute substantially to the total uncertainty and it also leads to a substantially reduced sensitivity to uncertainty in [BC]. Assuming 30% uncertainty in the BBOA and NOOA concentrations, 10% in the $b_{\text{abs,obs}}$, and 10% in the mixing-induced enhancement, the estimated absolute average uncertainty is 35% at 405 nm and 50% at 532 nm. At 870 nm the uncertainty is more difficult to estimate given the initial assumption that BrC is nonabsorbing. It is likely at least as large as the uncertainty at 532 nm, and 50% uncertainty is assumed in Figure 10 for MAC_{BBOA} at 870 nm and 100% for MAC_{NOOA} .

For BBOA at Fresno, the AAE values depend somewhat on the specific wavelength pair considered, with $\text{AAE}_{\text{BBOA},405-532\text{nm}} < \text{AAE}_{\text{BBOA},405-870\text{nm}} < \text{AAE}_{532-870\text{nm}}$ (Table 1), and a fit to the three wavelengths giving $\text{AAE}_{\text{BBOA}} = 3.04$. The $w_{\text{BBOA}} = 1.20$ for the 405–532 nm pair but is 1.79 from the fit over all three wavelengths. For NOOA at Fresno, there are only reliable results at two wavelengths (405 and 532 nm) available, with $\text{AAE}_{\text{NOOA}} = 4.81$ and $w = 3.67$ using these wavelength pairs. The NOOA exhibits a steeper wavelength dependence than the BBOA.

3.4.2.2. Interpretation and Comparison With Literature

The MAC_{BBOA} values determined here are slightly larger than the average determined by Zhang et al. (2016) for measurements made in wintertime Fresno in 2013, 2 years earlier than the current study ($0.6 \text{ m}^2/\text{g}$ in that study for the total BBOA compared to $0.84 \text{ m}^2/\text{g}$ here, both at 405 nm). Some of this difference is likely attributable to different analysis methods. Zhang et al. (2016) relied on Mie theory to extract the absorption by BrC, whereas the current approach is more directly observational. Thus, we suggest that Zhang et al.

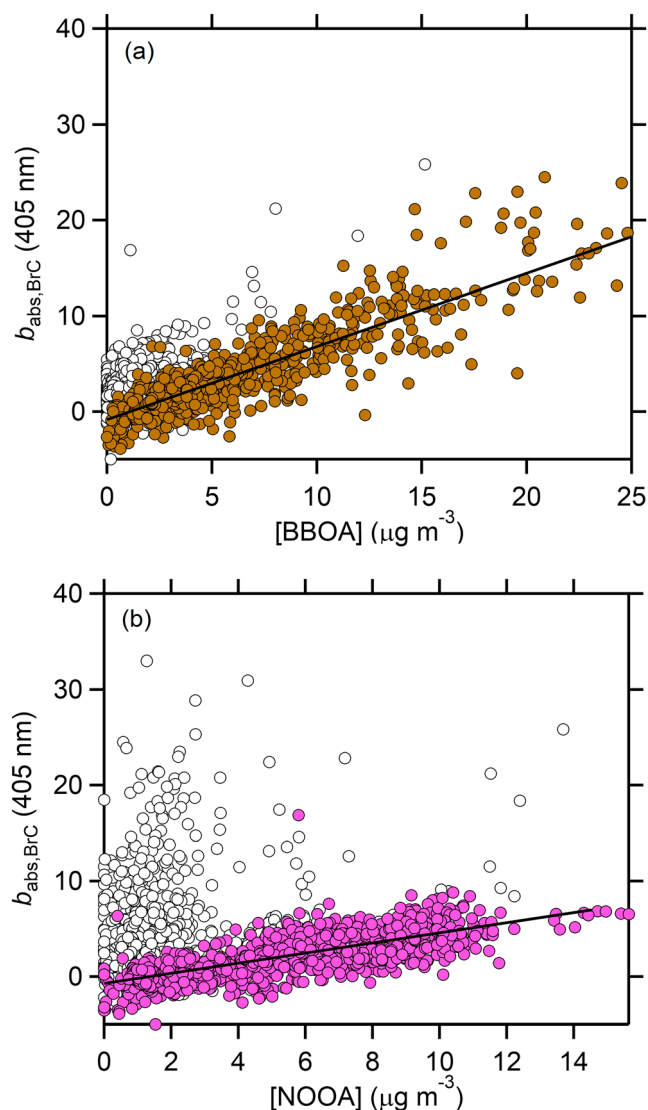


Figure 9. The relationship between absorption attributed to brown carbon at 405 nm and (a) the biomass burning organic aerosol (BBOA) factor and (b) the nitrate-associated organic aerosol (NOOA) factor for Fresno. In both panels the points are colored when the fraction of the factor was >20% and are white when the fraction of that factor was small. The black lines are linear fits, shown for reference.

(2016) likely underestimated the absorptivity of BBOA. In contrast to the current study, two BBOA factors were retrieved in 2013. Two OOA factors were also obtained, identified as a semivolatile OA (SV-OOA) and a low-volatility OA (LV-OOA; Young et al., 2016). However, Zhang et al. (2016) did not note any evidence for absorption by these other, non-BBOA factors. Thus, the finding that the NOOA is absorbing is new to this study. Reanalysis of the Zhang et al. (2016) data via multilinear regression using the *upper limit* approach (since there were no measurements of $R_{\text{coat-rBC}}$ available to allow estimation of the mixing-induced enhancement) indicates that one of the non-BBOA factors, the SV-OOA factor in that study, was likely somewhat absorbing, in addition to the BBOA factors. Consistent with Zhang et al. (2016), the multilinear regression indicates that one of their BBOA factors was more absorbing than the other, with $\text{MAC}_{\text{BBOA1}} = 0.79 \text{ m}^2/\text{g}$ and $\text{MAC}_{\text{BBOA2}} = 1.22 \text{ m}^2/\text{g}$ at 405 nm. The derived $\text{MAC}_{\text{BBOA1}}$ is quite similar to that obtained for the single BBOA factor from the current measurements. Their SV-OOA factor was much less absorbing than NOOA, with $\text{MAC}_{\text{SV-OOA}} = 0.14 \text{ m}^2/\text{g}$ at 405 nm. Most likely, the difference between the current study and Zhang et al. (2016) results from differences in environmental conditions, although we cannot rule out the possibility that there are differences in how the PMF analysis is splitting out the factors. In the current study, early morning fog was experienced during much of the study, especially in the latter half when NOOA concentrations were elevated. The ambient conditions were much colder and drier in Zhang et al. (2016), with little to no fog observed. This difference in behavior between these two studies strongly implicates fog, or at least wet aerosols, in the production of the light-absorbing chromophores that make NOOA BrC.

Given the preponderance of BBOA in the Fresno atmosphere it is tempting to implicate aqueous phase processing of biomass burning emissions as the source of absorbing NOOA (and SV-OOA). Gilardoni et al. (2016) suggested such a pathway as a major source of absorbing SOA in the Po Valley, Italy. However, the mass spectrum of NOOA (Chen et al., 2018) lacks a substantial peak at $m/z = 29$ that Gilardoni et al. (2016) indicated was a key signature of SOA produced from aqueous processing of biomass burning emissions. (The $m/z = 29$ peak is slightly larger for the SV-OOA from 2013; Young et al., 2016, but still much smaller than in Gilardoni et al., 2016.) Additionally, the NOOA factor is strongly correlated with particulate NO_3^- ($r^2 = 0.76$), and the diurnal profile of particulate nitrate, especially during the high-fog period, is strongly suggestive of substantial production of nitrate via nocturnal processing within the residual layer

(Prabhakar et al., 2017). Since most biomass burning emissions (from residential wood combustion) occur at night there is little that ends up in the residual layer, the composition of which is determined primarily by what is in the atmosphere just prior to sunset. Thus, our results do not support aqueous oxidation of biomass burning emissions as the predominant source of absorbing NOOA (and by extension, SV-OOA). Instead, we hypothesize that the absorptivity of NOOA here is a result of nitrate radical-related oxidation of organic compounds to produce organic nitrates that occurs in the residual layer at night; these organic nitrates may undergo further aqueous-phase processing that could contribute to BrC formation. While the exact production mechanism of the secondary BrC cannot be pinpointed, it seems likely that there is some role for aqueous phase processing coupled with nitrate-radical chemistry.

3.4.3. Fontana BrC

3.4.3.1. Observations

For Fontana, it is much less clear whether any of the OA factors are absorbing in nature at the wavelengths considered. The diurnal profiles of the derived $b_{\text{abs,BrC}}$ at 405 and 532 nm, excluding the fireworks impacted

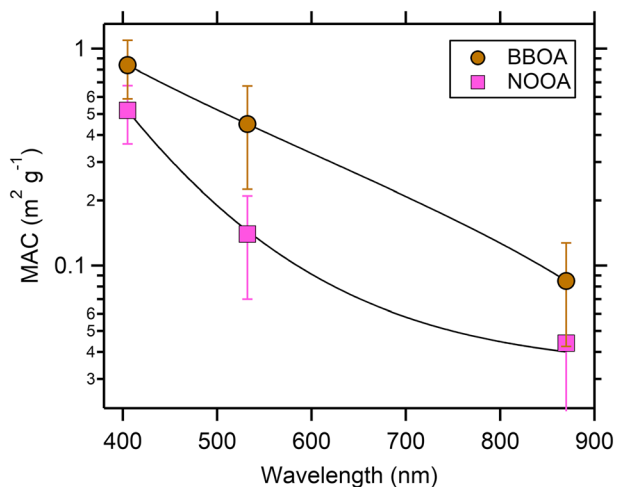


Figure 10. Variation of the organic aerosol (OA) factor-specific mass absorption coefficient (MAC) values for biomass burning OA (BBOA; brown circles) and nitrate-associated OA (NOOA; pink squares) with wavelength for Fresno. The lines are power law fits.

period, indicate a peak in $b_{\text{abs,BrC}}$ around 08:00 (local time; Figure 8). The $b_{\text{abs,BrC}}$ at 405 nm remains elevated throughout the afternoon, while the $b_{\text{abs,BrC}}$ at 532 nm falls to 0. Given that the $R_{\text{coat-rBC}}$ for this campaign shows a clear peak in the midafternoon (Lee et al., 2017), and since it has been assumed that all of the increase in the MAC_{BC} (and E_{abs}) with $R_{\text{coat-rBC}}$ at 532 nm results from mixing-induced enhancements, it is to be expected that the $b_{\text{abs,BrC}}$ at 532 nm is close to zero in the afternoon. The slightly elevated $b_{\text{abs,BrC}}$ at 405 nm in the afternoon could indicate that some photochemical production of BrC occurs, although it could be a limitation of the assumption that E_{abs} from mixing is wavelength independent. The afternoon organic composition is dominated by VOOA. A linear fit between $b_{\text{abs,BrC}}$ at 405 nm and VOOA has a slope of $0.04 \text{ m}^2/\text{g}$, although with a very low $r^2 < 0.01$, suggesting that VOOA is effectively nonabsorbing. This is further supported by considering that the $b_{\text{abs,BrC}}$ falls to near 0 at night, while the VOOA concentration, which peaks in the afternoon, is still elevated. Even if the upper limit approach is taken, such that all increases in E_{abs} are assumed to result from BrC with no contribution from a mixing-induced enhancement, the correlation between $b_{\text{abs,BrC}}$ and VOOA remains low ($r^2 = 0.07$). Thus, it seems reasonable to conclude that VOOA is primarily non-absorbing.

Considering the morning peak, comparison with the diurnal profiles of the OA factors (and the inorganic species and BC) provides some evidence that this peak in BrC absorption at Fontana is due to either NOOA or HOA. However, a multilinear fit against these species results in a very small combined r^2 value (≤ 0.16 for 405 nm, depending on what combination of OA factors is considered together). Further, the concentrations of NOOA and HOA are only slightly smaller at night than they are during the day, and thus, the lack of BrC absorption at night is inconsistent with these OA factors being absorbing. It may be that the time-dependent *missing mass* correction for [BC] did not sufficiently capture the diurnal variability in the correction to a level of precision required to assess the very small absorption over BC. Consequently, the observed noticeable, but ultimately small morning increase in $b_{\text{abs,BrC}}$ may simply be an analysis artifact. Regardless, the overall measurements suggest that the OA in Fontana is very weakly, if at all, absorbing, and thus, the contribution to the total absorption is small; the estimated fractional contribution of BrC to total absorption, excluding the fireworks-impacted period, is 0.03 at 405 nm and even smaller at 532 nm. Even at the peak $b_{\text{abs,BrC}}$ the BrC fractional contribution is only 10% of the total absorption.

3.4.3.2. Interpretation and Comparison With Literature

The observations for Fontana differ from previous measurements of absorption by water soluble organic carbon (WSOC) made in 2010 in both Pasadena, CA, and Riverside, CA, which are located in the same air basin as Fontana (Zhang, Lin, et al., 2011; Zhang et al., 2013). Zhang, Lin, et al. (2011) found that both $b_{\text{abs,WSOC}}$ and [WSOC] peaked in midafternoon and that they were correlated with a slope of $\sim 0.73 \text{ m}^2/\text{g}$ at 365 nm (for the Pasadena site). The measured absorption increased when samples were extracted from filters into methanol rather than water, and substantial absorption persisted to $>600 \text{ nm}$ for the methanol extracts (Zhang et al., 2013). If the VOOA here (which peaks in the afternoon) were as absorbing as the WSOC in the Zhang et al. studies, then the total absorption observed in Fontana should have been much larger and with a very different diurnal profile. Given the close proximity of Fontana and Riverside (20 km), it is difficult to reconcile the current observations, which suggest minimal absorption by the photochemically produced OA (specifically, VOOA), with the observations of Zhang et al. (2013) and Zhang, Lin, et al. (2011). A key difference between the measurement methods is that the current measurements were made in situ on dried particles, whereas the Zhang et al. measurements were made after extraction of particles into either water or methanol. It is possible that either the process of drying (here) or wetting (in Zhang et al., 2013; Zhang, Lin, et al., 2011) led to changes in the OA absorptivity. Some laboratory results indicate that drying can lead to rapid browning of OA (Nguyen et al., 2012). However, if this impacted the current measurements, then we would expect the OA to have appeared more absorbing than the extracted samples. In addition, the ambient RH was generally quite low, and thus, drying should have had minimal impact on particle water. It might be that extraction into water allowed reactions to occur that otherwise would not in the dry atmosphere.

3.4.4. BrC Refractive Indices

The determined MAC values can be used to calculate the imaginary refractive index via Mie theory for the absorbing OA types identified here. We limit this analysis to only the BBOA and NOOA factors identified in Fresno. In brief, the absorption coefficient is calculated using spherical particle Mie theory for a given size distribution and assumed imaginary refractive index (k) for the total particle. The theoretical MAC for a particle distribution can be calculated by dividing the calculated b_{abs} by the mass concentration of the distribution. Here BBOA- and NOOA-specific particle size distributions are used as input to the Mie model. There is a relationship between MAC and particle size for a given k . Thus, it is important to use a representative size distribution when inverting MAC values to k values. Factor-specific size distributions were determined as follows. Average number-weighted size distributions are determined from the SEMS over the period when the BBOA fraction was large (>0.15) and for when the NOOA fraction was large (>0.1). These distributions are then scaled by multiplying by the average BBOA or NOOA fraction during the appropriate period to produce BBOA- and NOOA-specific distributions. The factor-specific distributions are used as input to the Mie model. The density of the particles in the distribution is assumed size-independent and estimated from Kuwata et al. (2012) based on the AMS-measured O:C and H:C ratios (Chen et al., 2018). The assumed k is varied until the calculated MAC matches the observed component-specific MAC, resulting in the component-specific k (i.e., k_{BBOA} or k_{NOOA}). As the real refractive index (n) of the BrC components is not known a priori, a value of $n = 1.5$ is used. This is similar to that found for laboratory-generated secondary OA and to ammonium sulfate and ammonium nitrate. The likely uncertainty on the estimated n is ± 0.05 , which translates to an additional uncertainty on the estimated k of about 5%, as determined from sensitivity tests. The resulting derived k_{BBOA} are 0.024 ± 0.01 (405 nm), 0.018 ± 0.01 (532 nm), and 0.0068 ± 0.005 (870 nm). The k_{NOOA} are 0.012 ± 0.007 (405 nm) and 0.005 ± 0.003 (532 nm; see also Table 1). The uncertainties were estimated based on the uncertainty in the MAC_{BrC} values and the uncertainty in the assumed n . The comparable k values under the upper limit assumption are also provided in Table 1. The wavelength dependence of the k_{BBOA} and k_{NOOA} are calculated from equation (4). The $w_{\text{BBOA}} = 1.20$ for the 405–532 nm pair but is 1.65 from the fit over all three wavelengths. For NOOA at Fresno, there are only reliable results at two wavelengths (405 and 532 nm) available, giving $w = 3.67$. As already indicated by the wavelength dependence of the OA-type MAC values, the NOOA exhibits a steeper wavelength dependence than the BBOA.

4. Conclusions and Implications

The observations for two field campaigns in distinctly different urban environments (wintertime Fresno, CA, versus summertime Fontana, CA) here demonstrate that the magnitude of the mixing-induced absorption enhancement for BC (i.e., the lensing effect) is small for the ensemble-average absorption. Additionally, the absorption enhancement shows limited dependence on the ensemble-average coating-to-BC core ratio. These observations, considered with others (Cappa et al., 2012; Healy et al., 2015; Liu, Aiken, et al., 2015; McMeeking et al., 2014), demonstrate that spherical core-shell Mie theory calculations will not reliably give good agreement with observations when ensemble-average properties are considered, which is what is done in most climate models. This is the case because most models that consider internal mixing of BC assume that all components are internally mixed and do not account for only a small fraction of the NR-PM material being internally mixed with BC. For these two studies, only around 10–20% of NR-PM is internally mixed with BC. Thus, the amount of coating material is likely to be overestimated by models, and the mixing-induced absorption enhancement would be overestimated to an even greater extent. Instead, it is suggested that accounting for BC mixing-state diversity (i.e., differences in the composition between BC-containing particles, beyond whether a particle simply contains BC or not), such as has been done by Fierce et al. (2016), will be necessary to allow for accurate simulation of absorption by BC. While an empirical relationship between the mixing-induced E_{abs} for BC and $R_{\text{coat-rBC}}$ could be determined from the current observations, such a relationship is unlikely to be robust or generalizable, given differences observed around the world (Cappa et al., 2012; Healy et al., 2015; Liu, Aiken, et al., 2015; McMeeking et al., 2014).

For the Fresno observations, two types of BrC were identified and characterized: BBOA and NOOA. The BBOA, derived from residential wood combustion, was highly absorbing at 405 nm ($\text{MAC}_{\text{BBOA}} = 0.84 \text{ m}^2/\text{g}$) and the absorptivity persisted out to 870 nm ($\text{MAC}_{\text{BBOA}} = 0.085 \text{ m}^2/\text{g}$). The NOOA was less absorbing,

with $MAC_{NOOA} = 0.52 \text{ m}^2/\text{g}$ at 405 nm and absorption that was indistinguishable from zero at 870 nm. The NOOA was associated with the occurrence of heavy, early-morning fog and with an increased prevalence of particulate nitrate. The NOOA likely results from nitrate radical oxidation, coupled with aqueous processing. In the Fresno wintertime environment, the BBOA contribution (and associated absorption) was limited primarily to the nighttime, when surface emissions were high and the nocturnal boundary layer was low. Consequently, the local and regional radiative impacts of BBOA from residential wood combustion (and the co-emitted BC) are likely small because these are highly diluted into the daytime mixed boundary layer. In contrast, the NOOA concentration (and associated absorption) is greatest during the day. Thus, the NOOA may impact local and regional radiative forcing by increasing the daytime absorption of solar radiation. Also, since it seems likely that the NOOA is formed to a large extent by nocturnal chemical processing in the residual layer, the NOOA might exist above the ground-level fogs and could contribute to stabilization of the atmosphere and to fog persistence. In contrast to Fresno, there was little evidence of a notable contribution from BrC in summertime Fontana.

Appendix A: rBC Size Distribution Processing

The campaign-average mass-weighted BC size distributions derived from the SP2 for Fresno and Fontana are shown in Figure 3, along with the average size distribution for nighttime hours (19:00–07:00) and daytime hours (07:00–19:00). For Fresno, the observed campaign average distribution mode peak is around 150 nm. The size distribution mode is somewhat larger than this at nighttime, around 160 nm, and smaller during the daytime, around 130 nm. The size distribution can be seen to continuously shift from being dominated by the larger mode to being dominated by a smaller mode with time of day, as previously reported by Zhang et al. (2016) for this region. In addition, the observed size distributions all show evidence of an increase in concentration at diameters less than 100 nm. This upturn in concentration is especially apparent in the daytime size distributions, although is evident at all times of day. This strongly suggests that there is an additional mode that is located at a size below the SP2 detection window ($>80 \text{ nm}$). Although the presence of such a mode is not commonly noted in the literature, Liggio et al. (2012) reported measurements that also suggested a substantial small diameter mode, as did Zhang et al. (2016). Because these small-mode particles are below the SP2 detection window, the SP2 BC concentration measurements will be biased low. In addition, the concentration of particles at the upper limit of the SP2 (here, $\sim 800 \text{ nm}$) is greater than 0, indicating that particles at even larger sizes are contributing to the actual BC mass concentration. Accounting for such *missing mass* (i.e., mass contributed by particles outside the detection window) is important if the actual BC concentration is to be reasonably determined.

For Fontana, the mass-weighted size distribution mode occurs at a smaller diameter than in Fresno. Also, while there is still substantial diurnal variability in the BC concentration, the shape of the size distribution is quite constant throughout the day. As noted already, this difference between Fresno and Fontana is likely because in Fresno there are two major BC sources (vehicles and biomass burning), while in Fontana one source dominates (vehicles). As with Fresno, there is clear evidence of an increase in BC concentrations at diameters less than 100 nm, again suggesting the presence of a small mode that contributes substantially to the overall BC mass but that was not detected by the SP2.

One approach that has been taken to correct for the missing mass is to fit the campaign average size distribution with a lognormal distribution, and then to use this fit to extrapolate to larger and smaller sizes to estimate the fractional amount of missing mass (e.g., Schwarz et al., 2006). A constant scaling factor is then applied to the data set. However, such an approach is not appropriate here, since it is clear that at least for Fresno, the distribution shape is changing with time of day. This suggests, instead, that a temporally varying correction is required. Therefore, the approach taken here is to perform fits on 10-min average size distributions to determine a time-dependent missing mass correction. Also, instead of fitting the observations with a single lognormal distribution, the observations have been fit using the sum of four individual lognormal modes. Robust results were not obtained when fewer than four modes were used for either data set, although the use of 4 (rather than 3 or 2) was more important for Fresno than for Fontana.

Given that one of the modes peaks at a diameter below the measurement range, neither the exact position nor width of this mode is well constrained. To introduce consistency in the measurement method,

Table A1

The Mode Diameter, Width, and Average Mass Fraction Characterizing the Four Lognormal Modes Fit to the Observed Black Carbon Mass-Weighted Size Distributions

Note	Fresno			Fontana		
Mode	$d_{p,VED}$ (nm)	σ_g	Average mass fraction	$d_{p,VED}$ (nm)	σ_g	Average mass fraction
Mode 1	57	1.47	$0.37^{+0.11}_{-0.04}$	47	1.63	$0.52^{+0.13}_{-0.05}$
Mode 2	118	1.43	$0.23^{+0.01}_{-0.02}$	116	1.43	$0.26^{+0.02}_{-0.03}$
Mode 3	182	1.53	$0.21^{+0.05}_{-0.05}$	182	1.53	$0.12^{+0.03}_{-0.03}$
Mode 4	420	2.83	$0.19^{+0.01}_{-0.03}$	420	2.83	$0.10^{+0.01}_{-0.02}$

the exact position and width of each mode are set as a constant for each campaign. As the positions of these modes are not known a priori, the following approach is taken to determine an optimal value to use for each of the mode diameters. First, initial fits are performed wherein the position and width of each mode are constrained to fall within a range, but allowed to vary within this range. The ranges considered were as follows: Mode 1, $30 \text{ nm} < d_{p,VED} < 70 \text{ nm}$ and $1.2 < \sigma_g < 1.9$; Mode 2, $90 < d_{p,VED} < 140 \text{ nm}$ and $1.2 < \sigma_g < 1.9$; Mode 3, $150 < d_{p,VED} < 250 \text{ nm}$ and $1.3 < \sigma_g < 1.9$; and, Mode 4, $350 < d_{p,VED} < 500 \text{ nm}$ and $1.6 < \sigma_g < 3$. The average mode diameter and σ_g are then determined for each of the four modes based on initial fits to the campaign average size distributions. These are then used as constants in subsequent fitting to determine the time-dependent mode amplitudes. The optimal values used in the final, constrained fitting (where both the mode diameter, d_m , and σ_g , are held constant) for both campaigns are given in Table A1, along with the fractional contribution to the total mass of each mode. An attempt was made to maintain the mode positions and widths as campaign-independent constants, but it was determined that slight shifts in the position and width of the first two modes was necessary for optimal fitting.

Each of the 10-min average mass-weighted size distributions was fit with the constrained four-mode lognormal distribution, where the amplitude (i.e., concentration) of each peak is allowed to vary but the diameter and width are held constant. The results from this fitting are shown in Figure 3, where the fit results are compared with the observed size distributions and the diurnal variation in the mode-specific BC concentration is shown for each campaign.

The mode diameter and σ_g for Mode 1 are particularly uncertain, as this mode occurs below the lower size detection limit of the SP2. The average and standard deviation of the $d_{p,VED}$ and σ_g for Mode 1 for Fresno, for example, are $57 \pm 10 \text{ nm}$ and $1.47 \pm 0.14 (1\sigma)$. Uncertainty in the mode position and width for Mode 1 contributes to uncertainty in the absolute rBC mass attributed to this mode. In general, if the $d_{p,ved}$ is smaller the [rBC] for this mode increases, and vice versa. Larger changes in the Mode 1 [rBC] result from a decrease in $d_{p,ved}$ than from an increase. If the σ_g for Mode 1 is smaller, then the [rBC] and fractional abundance of Mode 1 is decreased slightly, and vice versa, although to a lesser extent than for changes in the mode diameter. However, uncertainty in the position and width lead to negligible changes in the diel variability that was determined for each mode. Thus, the qualitative conclusions are not impacted by uncertainty in the small-mode position or width.

The extent to which uncertainty in $d_{p,ved}$ and σ_g contribute to uncertainty in the overall [rBC] is quantified here by refitting the campaign average rBC size distribution from Fresno using $d_{p,ved} = 47 \text{ nm}$ and 67 nm or $\sigma_g = 1.33$ and 1.61 . We note that in all of these cases the χ^2 of the fit is larger—and the fit curve is visibly less good (Figure S9)—compared to when the campaign average $d_{p,ved}$ and σ_g are used, indicating that these alternate cases give lower quality fits. If $d_{p,VED} = 47 \text{ nm}$, rather than 57 nm , the Mode 1 [rBC] increases by 65% and if $d_{p,ved} = 67 \text{ nm}$ the Mode 1 [rBC] decreases by 25%. These changes are associated in changes in the abundance of rBC in the other modes. In general, for a decrease in $d_{p,ved}$ for Mode 1 the Mode 2 [rBC] increases slightly (by ~20%), the Mode 3 [rBC] decreases slightly (by ~5%), and the Mode 4 [rBC] is largely unaffected. The overall change in the [rBC] is an increase by 24% if $d_{p,ved} = 47 \text{ nm}$ and a decrease by 10% if $d_{p,ved} = 67 \text{ nm}$.

A decrease in σ_g to 1.33 for Mode 1 increases the Mode 1 [rBC] by 9%, while an increase to 1.61 decreases the Mode 1 [rBC] by 18%. The associated changes in [rBC] of the other modes for a decrease in σ_g to 1.33 are +30% (Mode 2), -8% (Mode 3), and +4% (Mode 4), and for an increase in σ_g to 1.61 are -37% (Mode 2), +3% (Mode 3), and -1% (Mode 4). In contrast to change in the Mode 1 $d_{p,ved}$, changes in σ_g do not lead to notable changes in the total [rBC] across modes, with [rBC] changing by only 2% for either an increase or decrease in the σ_g .

An increase in the [rBC] would correspond to a decrease in the calculated $MAC_{BC,ref}$ values by an equivalent amount, and vice versa. For example, if the [rBC] were 24% higher (the case if $d_{p,ved} = 47$ nm) the $MAC_{BC,ref}$ values would decrease to $3.3 \text{ m}^2/\text{g}$ (870 nm), $5.7 \text{ m}^2/\text{g}$ (532 nm), and $8.1 \text{ m}^2/\text{g}$ (405 nm). However, it is important to note that this would have limited impact on the derived absorption for BrC. This is because the BrC absorption is calculated as the difference between the observed absorption and the calculated BC absorption, with the latter being determined as the product of the $MAC_{BC,ref}$ and [rBC] (see equation (5)). Thus, an increase in the [rBC] would be offset by a corresponding decrease in the $MAC_{BC,ref}$ and the BrC absorption is not affected.

Appendix B: Comparison Between MAC-Based and Thermodenuder-Based Results for Absorption Enhancement

The absorption enhancement from the thermodenuder (TD) method is calculated as

$$E_{abs,TD} = \frac{2 \cdot MAC_{BC,t,amb}}{MAC_{BC,t-1,TD} + MAC_{BC,t+1,TD}} \quad (6)$$

where the subscript amb and TD refer to the ambient or thermodenuded measurements, respectively, and the $t - 1$ and $t + 1$ refer to the (5-min average) measurements made just before and after the measurement made at time t . The use of MAC_{BC} , as opposed to b_{abs} , corrects for transmission losses of BC through the TD. The $E_{abs,TD}$ values can be compared to the E_{abs} values determined from the MAC method (equation (2)) that were used in the primary analysis above, referred to now as $E_{abs,MAC}$. Ideally, the $E_{abs,TD}$ and $E_{abs,MAC}$ values would give equivalent results. However, potential biases in either can impact their comparability and ultimately any conclusions regarding the actual magnitude of the absorption enhancement. For the MAC-derived E_{abs} , biases in the estimated $MAC_{BC,ref}$ would cause the absolute value of $E_{abs,MAC}$ to be either too high or low. Given the need for the *missing-mass* correction for [BC], uncertainties or temporal or coating-dependent biases in this correction would potentially lead to an inaccurate assessment of the diurnal variability or the dependence of $E_{abs,MAC}$ on properties such as $R_{coat-rBC}$. For the TD-derived E_{abs} , incomplete evaporation of coatings could lead to a low bias in the measured E_{abs} . Inaccurate correction for transmission losses could lead to biases in the absolute $E_{abs,TD}$ or in the temporal variation. And there is a potential for charring of organics to occur in the TD, leading to the production of (non-ambient) BrC, that would decrease $E_{abs,TD}$.

The diurnal variability in $E_{abs,TD}$ and $E_{abs,MAC}$ are shown for both Fresno and Fontana in Figure B1. For Fresno, there is generally good agreement between the two methods in terms of the absolute values obtained, thus providing confidence in the overall conclusions. However, it is apparent that there is a more pronounced daytime bump in $E_{abs,MAC}$ than there is in $E_{abs,TD}$, in particular at 405 and 532 nm. If the low-fog and high-fog periods are considered separately (not shown), it becomes evident that the disagreement between the two methods is predominately limited to the high-fog period, especially at 405 and 532 nm, thus implicating the NOAA as a source of the difference. We hypothesize that the difference between methods for Fresno results from charring of the BrC from NOAA. Charring of NOAA and formation of absorbing material would lead to a suppression in the daytime $E_{abs,TD}$. However, the good agreement between methods during the low-fog period suggests that BBOA is not especially susceptible to charring and also that the missing-mass correction reasonably accounted for the diurnal variation in [BC]. Regardless, whether the $E_{abs,MAC}$ or $E_{abs,TD}$ is considered, it is apparent that the magnitude of E_{abs} at long wavelengths (here, 870 nm), where BrC contributions are relatively small, remains small throughout the campaign, supporting the conclusion that the mixing-induced enhancement is small.

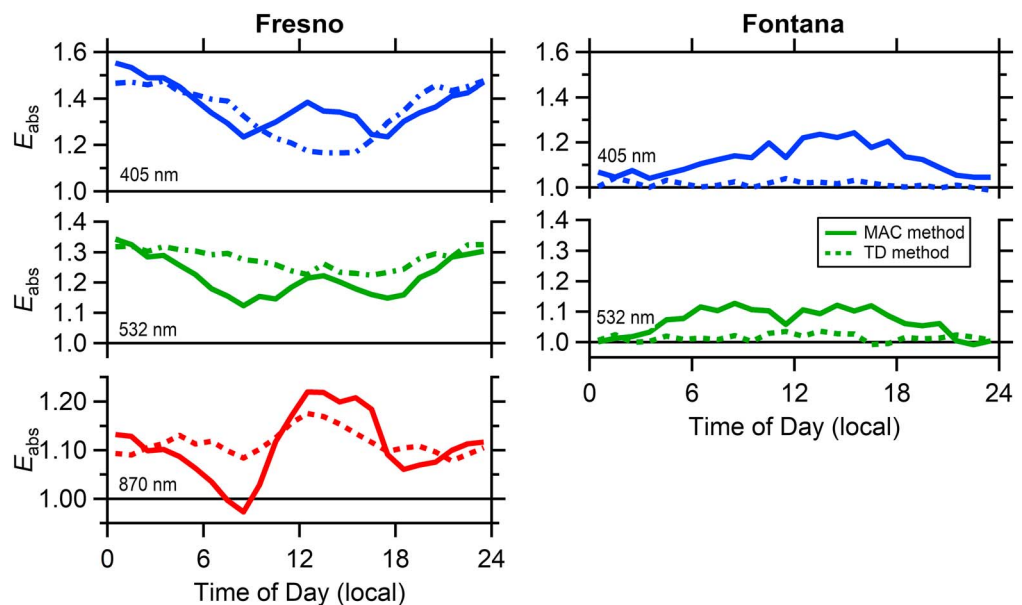


Figure B1. Campaign average diurnal variation in E_{abs} as calculated from the mass absorption coefficient (MAC)-method (solid lines) and the thermodenuder (TD)-method (dashed lines). Fresno results are on the left, Fontana on the right for (top-to-bottom) 405, 532, and 870 nm.

For Fontana, there is a more distinct difference between the two methods. While the diurnal variation in $E_{\text{abs,MAC}}$ shows a clear daytime maximum for both 405 and 532 nm, the $E_{\text{abs,TD}}$ is flat throughout the day and centered at 1 (indicating no enhancement; Figure B1). Correspondingly, the $E_{\text{abs,TD}}$ shows negligible dependence on $R_{\text{coat-rBC}}$, while the $E_{\text{abs,MAC}}$ increased to a small extent with $R_{\text{coat-rBC}}$ (Figure 5). Thus, it could be that residual coating material when $R_{\text{coat-rBC}}$ is high has biased the $E_{\text{abs,TD}}$ low. The ratio of the thermodenuded to ambient SP-AMS measurements can give an indication of the mass fraction of coating (MFR_{coat}) that remains after heating. The average MFR_{coat} for Fontana was 0.14. There was a distinct diurnal variation in MFR_{coat} , with the residual coating actually being smallest in the daytime when the $R_{\text{coat-rBC}}$ and $E_{\text{abs,MAC}}$ both peak. This observation indicates that evaporation of coating material was most efficient when the relative coating amount was greatest and thus suggests that residual coating material is not primarily responsible for the difference between methods. It is possible that charring of VOOA led to suppression of the $E_{\text{abs,TD}}$. However, the MFR for the total OA was only 0.06 with a negligible diurnal dependence, indicating that very little OA remained after heating. Thus, charring does not seem likely to be the primary reason for the difference between methods. Notably, the BC missing-mass fraction exhibits a diurnal variation that is similar to the observed $E_{\text{abs,MAC}}$ dependence (Figure 3 versus Figure B1). It is possible that the missing mass correction underestimated the amount of BC during the daytime, thus leading to an overestimate of the $E_{\text{abs,MAC}}$ and introducing an apparent dependence on $R_{\text{coat-rBC}}$ since $R_{\text{coat-rBC}}$ peaks during the daytime. If true, this would imply an even smaller-to-negligible dependence of E_{abs} on $R_{\text{coat-rBC}}$. Ultimately, the specific reason for the $E_{\text{abs,MAC}}$ and $E_{\text{abs,TD}}$ measurements cannot be discerned from the Fontana observations. However, both methods indicate that the E_{abs} in this region is small and that the dependence on $R_{\text{coat-rBC}}$ is very weak, and thus, the general conclusions reached are independent of which method is used. Based on the above discussion, it is strongly recommended that future experiments to measure E_{abs} in ambient employ multiple methods.

References

- Adachi, K., Chung, S. H., & Buseck, P. R. (2010). Shapes of soot aerosol particles and implications for their effects on climate. *Journal of Geophysical Research*, 115, D15206. <https://doi.org/10.1029/2009JD012868>
- Andreae, M. O., & Gelencser, A. (2006). Black carbon or brown carbon? The nature of light-absorbing carbonaceous aerosols. *Atmospheric Chemistry and Physics*, 6(10), 3131–3148. <https://doi.org/10.5194/acp-6-3131-2006>

Acknowledgments

The authors would like to acknowledge funding and support from California Air Resources Board (agreement 13-330) and contract manager Nehzat Motallebi. The authors would also like to thank the Fontana Fire Department and the South Coast Air Quality Management District for Fontana site logistics and UCD Extension for Fresno site logistics. Support for the Fontana SP-AMS measurements was provided by the Natural Sciences and Engineering Research Council of Canada (NSERC). Droplet Measurement Technologies provided the PAX for use during the Fresno campaign. The statements and conclusions in this paper are those of the researchers and not necessarily those of CARB. The mention of commercial products, their source, or their use in connection with material reported herein is not to be construed as actual or implied endorsement of such products. Measurement data from both campaigns are archived at the University of California, San Diego Library Digital Collections at <https://doi.org/10.6075/JOVX0DF9>.

- Betha, R., Russell, L. M., Chen, C.-L., Liu, J., Price, D. J., Sanchez, K. J., Chen, S., et al. (2018). Larger submicron particles for emissions with residential burning in wintertime San Joaquin Valley (Fresno) than for vehicle combustion in summertime South Coast Air Basin (Fontana). *Journal of Geophysical Research: Atmospheres*, *123*, 10,526–10,545. <https://doi.org/10.1029/2017JD026730>
- Bond, T. C., & Bergstrom, R. W. (2006). Light absorption by carbonaceous particles: An investigative review. *Aerosol Science and Technology*, *40*(1), 27–67. <https://doi.org/10.1080/02786820500421521>
- Bond, T. C., Habib, G., & Bergstrom, R. W. (2006). Limitations in the enhancement of visible light absorption due to mixing state. *Journal of Geophysical Research*, *111*, D20211. <https://doi.org/10.1029/2006JD007315>
- Bond, T. C., Doherty, S. J., Fahey, D. W., Forster, P. M., Berntsen, T., DeAngelo, B. J., Flanner, M. G., et al. (2013). Bounding the role of black carbon in the climate system: A scientific assessment. *Journal of Geophysical Research: Atmospheres*, *118*, 5380–5552. <https://doi.org/10.1002/jgrd.50171>
- Canagaratna, M. R., Jayne, J. T., Jimenez, J. L., Allan, J. D., Alfarra, M. R., Zhang, Q., Onasch, T. B., et al. (2007). Chemical and microphysical characterization of ambient aerosols with the Aerodyne aerosol mass spectrometer. *Mass Spectrometry Reviews*, *26*(2), 185–222. <https://doi.org/10.1002/mas.20115>
- Cappa, C. D., Onasch, T. B., Massoli, P., Worsnop, D. R., Bates, T. S., Cross, E. S., Davidovits, P., et al. (2012). Radiative absorption enhancements due to the mixing state of atmospheric black carbon. *Science*, *337*(6098), 1078–1081. <https://doi.org/10.1126/science.1223447>
- Chakrabarty, R. K., Moosmüller, H., Chen, L. W. A., Lewis, K., Arnott, W. P., Mazzoleni, C., Dubey, M. K., et al. (2010). Brown carbon in tar balls from smoldering biomass combustion. *Atmospheric Chemistry and Physics*, *10*(13), 6363–6370. <https://doi.org/10.5194/acp-10-6363-2010>
- Chen, C.-L., Chen, S., Russell, L. M., Liu, J., Price, D. J., Betha, R., Sanchez, K. J., et al. (2018). Organic aerosol particle chemical properties associated with residential burning and fog in wintertime San Joaquin Valley (Fresno) and with vehicle and firework emissions in summertime South Coast Air Basin (Fontana). *Journal of Geophysical Research: Atmospheres*, *123*, 10,707–10,731. <https://doi.org/10.1029/2018JD028374>
- Clarke, A., McNaughton, C., Kapustin, V., Shinozuka, Y., Howell, S., Dibb, J., Zhou, J., et al. (2007). Biomass burning and pollution aerosol over North America: Organic components and their influence on spectral optical properties and humidification response. *Journal of Geophysical Research*, *112*, D12S18. <https://doi.org/10.1029/2006JD007777>
- Collier, S., Williams, L. R., Onasch, T. B., Cappa, C. D., Zhang, X., Russell, L. M., Chen, C.-L., et al. (2018). Influence of emissions and aqueous processing on particles containing black carbon in a polluted urban environment: Insights from a soot particle-aerosol mass spectrometer. *Journal of Geophysical Research: Atmospheres*, *123*, 6648–6666. <https://doi.org/10.1002/2017JD027851>
- Cross, E. S., Onasch, T. B., Ahern, A., Wrobel, W., Slowik, J. G., Olfert, J., Lack, D. A., et al. (2010). Soot particle studies—Instrument intercomparison—Project overview. *Aerosol Science and Technology*, *44*(8), 592–611. <https://doi.org/10.1080/02786826.2010.482113>
- Docherty, K. S., Stone, E. A., Ulbrich, I. M., DeCarlo, P. F., Snyder, D. C., Schauer, J. J., Peltier, R. E., et al. (2008). Apportionment of primary and secondary organic aerosols in Southern California during the 2005 Study of Organic Aerosols in Riverside (SOAR-1). *Environmental Science & Technology*, *42*(20), 7655–7662. <https://doi.org/10.1021/es8008166>
- Feng, Y., Ramanathan, V., & Kotamarthi, V. R. (2013). Brown carbon: A significant atmospheric absorber of solar radiation? *Atmospheric Chemistry and Physics*, *13*(17), 8607–8621. <https://doi.org/10.5194/acp-13-8607-2013>
- Fierce, L., Bond, T. C., Bauer, S. E., Mena, F., & Riemer, N. (2016). Black carbon absorption at the global scale is affected by particle-scale diversity in composition. *Nature Communications*, *7*(1), 12361. <https://doi.org/10.1038/ncomms12361>
- Forestieri, S. D., Helgestad, T. M., Lambe, A. T., Renbaum-Wolff, L., Lack, D. A., Massoli, P., Cross, E. S., et al. (2018). Measurement and modeling of the multi-wavelength optical properties of uncoated flame-generated soot. *Atmospheric Chemistry and Physics*, *18*(16), 12,141–12,159. <https://doi.org/10.5194/acp-18-12141-2018>
- Forrister, H., Liu, J., Scheuer, E., Dibb, J., Ziemba, L., Thornhill, K. L., Anderson, B., et al. (2015). Evolution of brown carbon in wildfire plumes. *Geophysical Research Letters*, *42*, 4623–4630. <https://doi.org/10.1002/2015GL063897>
- Fuller, K. A., Malm, W. C., & Kreidenweis, S. M. (1999). Effects of mixing on extinction by carbonaceous particles. *Journal of Geophysical Research*, *104*(D13), 15,941–15,954. <https://doi.org/10.1029/1998JD100069>
- Ge, X., Setyan, A., Sun, Y., & Zhang, Q. (2012). Primary and secondary organic aerosols in Fresno, California during wintertime: Results from high resolution aerosol mass spectrometry. *Journal of Geophysical Research*, *117*, D19301. <https://doi.org/10.1029/2012JD018026>
- Gilardoni, S., Massoli, P., Paglione, M., Giulianelli, L., Carbone, C., Rinaldi, M., Decesari, S., et al. (2016). Direct observation of aqueous secondary organic aerosol from biomass-burning emissions. *Proceedings of the National Academy of Sciences of the United States of America*, *113*(36), 10,013–10,018. <https://doi.org/10.1073/pnas.1602212113>
- Hayes, P. L., Ortega, A. M., Cubison, M. J., Froyd, K. D., Zhao, Y., Cliff, S. S., Hu, W. W., et al. (2013). Organic aerosol composition and sources in Pasadena, California, during the 2010 CalNex campaign. *Journal of Geophysical Research: Atmospheres*, *118*, 9233–9257. <https://doi.org/10.1002/jgrd.50530>
- Healy, R., Wang, J., Jeong, C. H., Lee, A., Willis, M., Jaroudi, E., Zimmerman, N., et al. (2015). Light-absorbing properties of ambient black carbon and brown carbon from fossil fuel and biomass burning sources. *Journal of Geophysical Research: Atmospheres*, *120*, 6619–6633. <https://doi.org/10.1002/2015JD023382>
- Kirchstetter, T. W., Novakov, T., & Hobbs, P. V. (2004). Evidence that the spectral dependence of light absorption by aerosols is affected by organic carbon. *Journal of Geophysical Research*, *109*, D21208. <https://doi.org/10.1029/2004JD004999>
- Knox, A., Evans, G. J., Brook, J. R., Yao, X., Jeong, C. H., Godri, K. J., Sabaliauskas, K., et al. (2009). Mass absorption Cross-section of ambient black carbon aerosol in relation to chemical age. *Aerosol Science and Technology*, *43*(6), 522–532. <https://doi.org/10.1080/02786820902777207>
- Kondo, Y., Matsui, H., Moteki, N., Sahu, L., Takegawa, N., Kajino, M., Zhao, Y., et al. (2011). Emissions of black carbon, organic, and inorganic aerosols from biomass burning in North America and Asia in 2008. *Journal of Geophysical Research*, *116*, D08204. <https://doi.org/10.1029/2010JD015152>
- Krasowsky, T. S., McMeeking, G. R., Wang, D. B., Sioutas, C., & Ban-Weiss, G. A. (2016). Measurements of the impact of atmospheric aging on physical and optical properties of ambient black carbon particles in Los Angeles. *Atmospheric Environment*, *142*, 496–504. <https://doi.org/10.1016/j.atmosenv.2016.08.010>
- Kuwata, M., Zorn, S. R., & Martin, S. T. (2012). Using elemental ratios to predict the density of organic material composed of carbon, hydrogen, and oxygen. *Environmental Science & Technology*, *46*(2), 787–794. <https://doi.org/10.1021/es202525q>
- Lack, D. A., & Cappa, C. D. (2010). Impact of brown and clear carbon on light absorption enhancement, single scatter albedo and absorption wavelength dependence of black carbon. *Atmospheric Chemistry and Physics*, *10*(9), 4207–4220. <https://doi.org/10.5194/acp-10-4207-2010>

- Lack, D. A., Cappa, C. D., Cross, E. S., Massoli, P., Ahern, A. T., Davidovits, P., & Onasch, T. B. (2009). Absorption enhancement of coated absorbing aerosols: Validation of the photo-acoustic technique for measuring the enhancement. *Aerosol Science and Technology*, *43*(10), 1006–1012. <https://doi.org/10.1080/02786820903117932>
- Lack, D. A., Langridge, J., Bahreni, R., Cappa, C. D., Middlebrook, A., & Schwarz, J. P. (2012). Brown carbon and internal mixing in biomass burning particles. *Proceedings of the National Academy of Sciences of the United States of America*, *109*(37), 14,802–14,807. <https://doi.org/10.1073/pnas.1206575109>
- Lack, D. A., & Langridge, J. M. (2013). On the attribution of black and brown carbon light absorption using the Ångström exponent. *Atmospheric Chemistry and Physics*, *13*(20), 10,535–10,543. <https://doi.org/10.5194/acp-13-10535-2013>
- Lack, D. A., Moosmüller, H., McMeeking, G. R., Chakrabarty, R. K., & Baumgardner, D. (2014). Characterizing elemental, equivalent black, and refractory black carbon aerosol particles: A review of techniques, their limitations and uncertainties. *Analytical and Bioanalytical Chemistry*, *406*(1), 99–122. <https://doi.org/10.1007/s00216-013-7402-3>
- Lack, D. A., Richardson, M. S., Law, D., Langridge, J. M., Cappa, C. D., McLaughlin, R. J., & Murphy, D. M. (2012). Aircraft instrument for comprehensive characterization of aerosol optical properties. Part 2: Black and brown carbon absorption and absorption enhancement measured with photo acoustic spectroscopy. *Aerosol Science and Technology*, *46*(5), 555–568. <https://doi.org/10.1080/02786826.2011.645955>
- Langridge, J. M., Richardson, M. S., Lack, D., Law, D., & Murphy, D. M. (2011). Aircraft instrument for comprehensive characterization of aerosol optical properties, part I: Wavelength-dependent optical extinction and its relative humidity dependence measured using cavity ringdown spectroscopy. *Aerosol Science and Technology*, *45*(11), 1305–1318. <https://doi.org/10.1080/02786826.2011.592745>
- Lee, A. K. Y., Chen, C. L., Liu, J., Price, D. J., Betha, R., Russell, L. M., Zhang, X., et al. (2017). Formation of secondary organic aerosol coating on black carbon particles near vehicular emissions. *Atmospheric Chemistry and Physics*, *17*(24), 15,055–15,067. <https://doi.org/10.5194/acp-17-15055-2017>
- Lee, A. K. Y., Willis, M. D., Healy, R. M., Onasch, T. B., & Abbatt, J. P. D. (2015). Mixing state of carbonaceous aerosol in an urban environment: Single particle characterization using the soot particle aerosol mass spectrometer (SP-AMS). *Atmospheric Chemistry and Physics*, *15*(4), 1823–1841. <https://doi.org/10.5194/acp-15-1823-2015>
- Lee, A. K. Y., Willis, M. D., Healy, R. M., Wang, J. M., Jeong, C. H., Wenger, J. C., Evans, G. J., et al. (2016). Single-particle characterization of biomass burning organic aerosol (BBOA): Evidence for non-uniform mixing of high molecular weight organics and potassium. *Atmospheric Chemistry and Physics*, *16*(9), 5561–5572. <https://doi.org/10.5194/acp-16-5561-2016>
- Lewis, K., Arnott, W. P., Moosmüller, H., & Wold, C. E. (2008). Strong spectral variation of biomass smoke light absorption and single scattering albedo observed with a novel dual-wavelength photoacoustic instrument. *Journal of Geophysical Research*, *113*, D16203. <https://doi.org/10.1029/2007JD009699>
- Liggio, J., Gordon, M., Smallwood, G., Li, S. M., Stroud, C., Staebler, R., Lu, G., et al. (2012). Are emissions of black carbon from gasoline vehicles underestimated? Insights from near and on-road measurements. *Environmental Science & Technology*, *46*(9), 4819–4828. <https://doi.org/10.1021/es2033845>
- Lim, S., Lee, M., Kim, S. W., & Laj, P. (2018). Sulfate alters aerosol absorption properties in East Asian outflow. *Scientific Reports*, *8*(1), 5172. <https://doi.org/10.1038/s41598-018-23021-1>
- Liu, D. T., Taylor, J. W., Young, D. E., Flynn, M. J., Coe, H., & Allan, J. D. (2015). The effect of complex black carbon microphysics on the determination of the optical properties of brown carbon. *Geophysical Research Letters*, *42*, 613–619. <https://doi.org/10.1002/2014gl062443>
- Liu, D. T., Whitehead, J., Alfarra, M., Reyes Villegas, E., Spracklen, D., Reddington, C. L., et al. (2017). Black-carbon absorption enhancement in the atmosphere determined by particle mixing state. *Nature Geoscience*, *10*(3), 184–188. <https://doi.org/10.1038/ngeo2901>
- Liu, J., Bergin, M., Guo, H., King, L., Kotra, N., Edgerton, E., & Weber, R. J. (2013). Size-resolved measurements of brown carbon in water and methanol extracts and estimates of their contribution to ambient fine-particle light absorption. *Atmospheric Chemistry and Physics*, *13*(24), 12,389–12,404. <https://doi.org/10.5194/acp-13-12389-2013>
- Liu, J., Scheuer, E., Dibb, J., Diskin, G. S., Ziemba, L. D., Thornhill, K. L., Anderson, B. E., et al. (2015). Brown carbon aerosol in the North American continental troposphere: Sources, abundance, and radiative forcing. *Atmospheric Chemistry and Physics*, *15*(14), 7841–7858. <https://doi.org/10.5194/acp-15-7841-2015>
- Liu, S., Aiken, A. C., Gorkowski, K., Dubey, M. K., Cappa, C. D., Williams, L. R., Herndon, S. C., et al. (2015). Enhanced light absorption by mixed source black and brown carbon particles in UK winter. *Nature Communications*, *6*(1), 8435. <https://doi.org/10.1038/ncomms9435>
- Massoli, P., Onasch, T. B., Cappa, C. D., Nuumaan, I., Hakala, J., Hayden, K., Li, S. M., et al. (2015). Characterization of black carbon-containing particles from soot particle aerosol mass spectrometer measurements on the R/V Atlantis during CalNex 2010. *Journal of Geophysical Research: Atmospheres*, *120*, 2575–2593. <https://doi.org/10.1002/2014JD022834>
- McMeeking, G. R., Fortner, E., Onasch, T. B., Taylor, J. W., Flynn, M., Coe, H., & Kreidenweis, S. M. (2014). Impacts of nonrefractory material on light absorption by aerosols emitted from biomass burning. *Journal of Geophysical Research: Atmospheres*, *119*, 12,272–12,286. <https://doi.org/10.1002/2014jd021750>
- Metcalf, A. R., Loza, C. L., Coggon, M. M., Craven, J. S., Jonsson, H. H., Flagan, R. C., & Seinfeld, J. H. (2013). Secondary organic aerosol coating formation and evaporation: Chamber studies using black carbon seed aerosol and the single-particle soot photometer. *Aerosol Science and Technology*, *47*(3), 326–347. <https://doi.org/10.1080/02786826.2012.750712>
- Nguyen, T. B., Lee, P. B., Updyke, K. M., Bones, D. L., Laskin, J., Laskin, A., & Nizkorodov, S. A. (2012). Formation of nitrogen- and sulfur-containing light-absorbing compounds accelerated by evaporation of water from secondary organic aerosols. *Journal of Geophysical Research*, *117*, D01207. <https://doi.org/10.1029/2011JD016944>
- Onasch, T. B., Trimborn, A. M., Fortner, E. C., Jayne, J. T., Kok, G. L., Williams, L. R., Davidovits, P., et al. (2012). Soot particle aerosol mass spectrometer: Development, validation and initial application. *Aerosol Science and Technology*, *46*(7), 804–817. <https://doi.org/10.1080/02786826.2012.663948>
- Peng, J., Hu, M., Guo, S., du, Z., Zheng, J., Shang, D., Levy Zamora, M., et al. (2016). Markedly enhanced absorption and direct radiative forcing of black carbon under polluted urban environments. *Proceedings of the National Academy of Sciences of the United States of America*, *113*(16), 4266–4271. <https://doi.org/10.1073/pnas.1602310113>
- Prabhakar, G., Parworth, C. L., Zhang, X., Kim, H., Young, D. E., Beyersdorf, A. J., Ziemba, L. D., et al. (2017). Observational assessment of the role of nocturnal residual-layer chemistry in determining daytime surface particulate nitrate concentrations. *Atmospheric Chemistry and Physics*, *17*(23), 14,747–14,770. <https://doi.org/10.5194/acp-17-14747-2017>
- Ramanathan, V., & Carmichael, G. (2008). Global and regional climate changes due to black carbon. *Nature Geoscience*, *1*(4), 221–227. <https://doi.org/10.1038/ngeo156>

- Saleh, R., Hennigan, C. J., McMeeking, G. R., Chuang, W. K., Robinson, E. S., Coe, H., Donahue, N. M., et al. (2013). Absorptivity of brown carbon in fresh and photo-chemically aged biomass-burning emissions. *Atmospheric Chemistry and Physics*, *13*(15), 7683–7693. <https://doi.org/10.5194/acp-13-7683-2013>
- Saleh, R., Robinson, E. S., Tkacik, D. S., Ahern, A. T., Liu, S., Aiken, A. C., Sullivan, R. C., et al. (2014). Brownness of organics in aerosols from biomass burning linked to their black carbon content. *Nature Geoscience*, *7*(9), 647–650. <https://doi.org/10.1038/ngeo2220>
- Scarnato, B. V., Vahidinia, S., Richard, D. T., & Kirchstetter, T. W. (2013). Effects of internal mixing and aggregate morphology on optical properties of black carbon using a discrete dipole approximation model. *Atmospheric Chemistry and Physics*, *13*(10), 5089–5101. <https://doi.org/10.5194/acp-13-5089-2013>
- Schnaiter, M., Linke, C., Mohler, O., Naumann, K. H., Saathoff, H., Wagner, R., Schurath, U., et al. (2005). Absorption amplification of black carbon internally mixed with secondary organic aerosol. *Journal of Geophysical Research*, *110*, D019204. <https://doi.org/10.1029/2005JD006046>
- Schwarz, J. P., Gao, R. S., Fahey, D. W., Thomson, D. S., Watts, L. A., Wilson, J. C., Reeves, J. M., et al. (2006). Single-particle measurements of midlatitude black carbon and light-scattering aerosols from the boundary layer to the lower stratosphere. *Journal of Geophysical Research*, *111*, D16207. <https://doi.org/10.1029/2006JD007076>
- Schwarz, J. P., Spackman, J. R., Gao, R. S., Perring, A. E., Cross, E., Onasch, T. B., Ahern, A., et al. (2010). The detection efficiency of the single particle soot photometer. *Aerosol Science and Technology*, *44*(8), 612–628. <https://doi.org/10.1080/02786826.2010.481298>
- Shiraiwa, M., Kondo, Y., Iwamoto, T., & Kita, K. (2010). Amplification of light absorption of black carbon by organic coating. *Aerosol Science and Technology*, *44*(1), 46–54. <https://doi.org/10.1080/02786820903357686>
- Tasoglou, A., Saliba, G., Subramanian, R., & Pandis, S. N. (2017). Absorption of chemically aged biomass burning carbonaceous aerosol. *Journal of Aerosol Science*, *113*, 141–152. <https://doi.org/10.1016/j.jaerosci.2017.07.011>
- Wang, X., Heald, C. L., Ridley, D. A., Schwarz, J. P., Spackman, J. R., Perring, A. E., Coe, H., et al. (2014). Exploiting simultaneous observational constraints on mass and absorption to estimate the global direct radiative forcing of black carbon and brown carbon. *Atmospheric Chemistry and Physics*, *14*(20), 10,989–11,010. <https://doi.org/10.5194/acp-14-10989-2014>
- Willis, M. D., Healy, R. M., Riemer, N., West, M., Wang, J. M., Jeong, C.-H., Wenger, J. C., et al. (2016). Quantification of black carbon mixing state from traffic: Implications for aerosol optical properties. *Atmospheric Chemistry and Physics*, *16*(7), 4693–4706. <https://doi.org/10.5194/acp-16-4693-2016>
- Willis, M. D., Lee, A. K. Y., Onasch, T. B., Fortner, E. C., Williams, L. R., Lambe, A. T., Worsnop, D. R., et al. (2014). Collection efficiency of the soot-particle aerosol mass spectrometer (SP-AMS) for internally mixed particulate black carbon. *Atmospheric Measurement Techniques*, *7*(12), 4507–4516. <https://doi.org/10.5194/amt-7-4507-2014>
- Young, D. E., Kim, H., Parworth, C., Zhou, S., Zhang, X., Cappa, C. D., Seco, R., et al. (2016). Influences of emission sources and meteorology on aerosol chemistry in a polluted urban environment: Results from DISCOVER-AQ California. *Atmospheric Chemistry and Physics*, *16*(8), 5427–5451. <https://doi.org/10.5194/acp-16-5427-2016>
- Zhang, Q., Jimenez, J. L., Canagaratna, M. R., Ulbrich, I. M., Ng, N. L., Worsnop, D. R., & Sun, Y. L. (2011). Understanding atmospheric organic aerosols via factor analysis of aerosol mass spectrometry: A review. *Analytical and Bioanalytical Chemistry*, *401*(10), 3045–3067. <https://doi.org/10.1007/s00216-011-5355-y>
- Zhang, X., Kim, H., Parworth, C., Young, D. E., Zhang, Q., Metcalf, A. R., & Cappa, C. D. (2016). Optical properties of wintertime aerosols from residential wood burning in Fresno, CA: Results from DISCOVER-AQ 2013. *Environmental Science & Technology*, *50*(4), 1681–1690. <https://doi.org/10.1021/acs.est.5b04134>
- Zhang, X., Lin, Y.-H., Surratt, J. D., & Weber, R. J. (2013). Sources, composition and absorption Ångström exponent of light-absorbing organic components in aerosol extracts from the Los Angeles Basin. *Environmental Science & Technology*, *47*(8), 3685–3693. <https://doi.org/10.1021/es305047b>
- Zhang, X. L., Lin, Y. H., Surratt, J. D., Zotter, P., Prevot, A. S. H., & Weber, R. J. (2011). Light-absorbing soluble organic aerosol in Los Angeles and Atlanta: A contrast in secondary organic aerosol. *Geophysical Research Letters*, *38*, L21810. <https://doi.org/10.1029/2011GL049385>
- Zhang, Y. X., Zhang, Q., Cheng, Y. F., Su, H., Li, H. Y., Li, M., Zhang, X., et al. (2018). Amplification of light absorption of black carbon associated with air pollution. *Atmospheric Chemistry and Physics*, *18*(13), 9879–9896. <https://doi.org/10.5194/acp-18-9879-2018>